CHAPTER 2

The Structural Geology of the Strangways Metamorphic Complex

Summary

Five deformations (D_1-D_5) involved in two deformation cycles have been recognized in rocks from the Strangways Metamorphic Complex. D_1 and D_2 produced layer-parallel foliations, with many of the effects of D_1 overprinted by non-coaxial shear during D_2. D_1 and D_2 form the first deformation cycle, which is called the *Strangways Event*. D_1 was synchronous with peak granulite facies metamorphism, which took place at about 1800 Ma; it produced an S_1 foliation preserved as inclusion trails in porphyroblasts and thin two-pyroxene mesosomes in folded migmatitic mafic lenses. A penetrative leucosome foliation (S_2) was produced during D_2 and was accompanied by the intrusion of charnockite and mafic dykes. Dating of zircons from a charnockite body indicates that D_2 occurred at 1765±4 Ma. Pegmatite bodies that partially transgress S_2 crystallized from partial melts as D_2 waned and temperature decreased. A major progressive deformational cycle (D_3-D_5) occurred after D_1-D_2 along a northeast axis. This deformational cycle is called the *Arunta Orogeny*. Dating of zircons from the syntectonic Anamarra granite indicates that D_3 occurred at 1745±4 Ma. Early D_3 deformation is characterized by tight to isoclinal, non-cylindrical F_3 folds, which resemble mylonitic folds. F_3 folds are associated with a well-developed stretching lineation (L_3) oriented parallel to the fold axes. Colinear, open, asymmetrical F_4 folds refold F_3. Conjugate crenulations on the limbs of F_4 folds and extensive dextral and sinistral shear zones, which formed late in D_3 indicate coaxial northeast-southwest shortening. Ultramylonitization with a normal sense of shear and local shear folding occurred during D_4. The principal extension direction during D_4 was parallel to D_3 fold axes. The effects of D_4 represent the partitioning of strain into local zones of non-coaxial deformation during the later stages of the deformational cycle. D_5 is characterized by deformation in wide shear zones, which preserve evidence for northeast over southwest sense of shear. The predominance of symmetrical porphyroclasts in D_5 zones suggests that the later part of the second deformational cycle may have been accommodated by a flattening-style strain.

2.1 Introduction

Complexly deformed mafic and felsic gneisses and less common supracrustal rocks, together with discordant orthogneisses, comprise the early-Proterozoic Strangways Metamorphic Complex, and crop out in the Central Tectonic Province (Shaw et al., 1984a) of the Arunta Block (Fig. 1.0). The Strangways Metamorphic Complex is thought to record a crustal formation Nd-Sm model age of about 2000 Ma (Windrim and McCulloch, 1986) and the earliest granulite facies metamorphic event in the Arunta Block (~ 1800Ma), called the Strangways Event (Black et al., 1983). The Strangways Metamorphic Complex was metamorphosed to granulite facies conditions and complexly deformed before being extensively dissected by mylonite and retrograde shear zones (Shaw et al., 1979, 1984b; Shaw and Langworthy, 1984; Norman and Clarke, 1990; Norman and Vernon, 1991; Chapter 3, Chapter 5). Warren (1983a, 1983b) inferred near-isobaric cooling to a normal continental geotherm from the metamorphic peak. Shaw et al. (1984a) briefly discussed the Proterozoic tectonometamorphic history of the Strangways Range and recognized three phases of folding prior to granulite facies metamorphism. However, a second distinct granulite facies metamorphism (M_2) has been recognized in rocks from the Strangways Metamorphic Complex (Iyer et al, 1976; Norman and Clarke, 1990; Chapter 3), which has been attributed to a major deformation event after the metamorphic peak. This deformation event is described in this Chapter.

Isotopic dates give conflicting interpretations on the age of the second granulite facies metamorphism (M_2) and subsequent deformation in the shear zones that bound the Strangways Metamorphic Complex. Rb/Sr and $^{40}Ar/^{39}Ar$ data suggest that major disturbances to the isotopic system occurred between 1450 and 1470 Ma ago (Iyer et al., 1976; Woodford et al., 1975) and this is the preferred age for the thermal pulse that produced M_2. However, U/Pb zircon studies (Mortimer et al., 1987; Cooper et al., 1988) suggest that intense shearing occurred at about 1750 Ma and that no further isotopic disturbances of the system occurred until 500 Ma.

In this Chapter, the structural evolution of gneisses is described from two smaller morphological units in the Strangways Metamorphic Complex: the *Ongeva granulites* (Shaw et al., 1984a) to the east and the *Anamarra granite domain* (Norman and Clarke, 1990) to the west and north (Fig. 1.1). Tectonic events in the two units are correlated where appropriate. D_1 and D_2 deformation resulted in layer-parallel foliations prior to D_3. The macroscopic compositional layering in the Strangways Metamorphic Complex strikes mainly northwest-southeast and dips at high to moderate angles to the east. The layering is folded into a complex pattern of dominant north to northeast plunging folds, which are attributed to a major multiple folding event (D_3), which post-dated peak metamorphism. South-east trending shear zones (D_4-D_5) cut and displace the folded compositional layering. The shear zone deformation may represent a continuation of a major deformation cycle that produced D_3 folding. The main macroscopic folding event is interpreted as a progressive non-coaxial deformation at granulite facies conditions and is probably equivalent to the ductile "Proterozoic reworking" of Goscombe (1991) in rocks from the Strangways Range, 75 km northwest of this study. The Strangways Metamorphic Complex is characterized by a consistent colinearity of stretching lineations (measured on the folded gneissosity), fold axes, ultramylonitic stretching lineations and mineral elongations in mylonite zones that bound the complex. The term *Arunta Orogeny* is introduced to refer to this major tectonic event. The term "Arunta Orogeny" has previously been used for the main granulite facies event (Allen and Stubbs, 1982), which was subsequently referred to as the *Strangways Event* (Black et al., 1983). In this Chapter, the Strangways Event is probably equivalent to D_1 and D_2 and the Arunta Orogeny refers only to the second major tectonothermal event, which was quite distinct from processes responsible for the main granulite facies event.

2.2 Ongeva granulites

The Ongeva granulites (Fig. 1.1) are mostly composed of interlayered granulite facies mafic and felsic gneisses and granofelses, which are transected by numerous high-grade shear zones. They are similar to other rocks in the Strangways Metamorphic

Complex, which have been interpreted as a metamorphosed bimodal suite of volcanics (Shaw et al., 1979; Warren and Shaw, 1985).

2.21 D_1/M_1 event

The Ongeva granulites consist of interlayered quartz-feldspar±orthopyroxene±garnet-biotite gneisses, two pyroxene-hornblende-plagioclase granofelses, quartz-K-feldspar-sillimanite-garnet-biotite gneisses and minor calc-silicate rocks and marble. A variation in bulk rock composition throughout the Ongeva granulites is observed on a cm to m-scale. Although the bulk compositional layering is generally 1-5 m thick, massive felsic granofels layers up to 100 m thick may occur (e.g. Mount Schaber granofels). Mafic gneisses and granofelses comprise about 50% of the outcrop and may also form thick massive layers. These lithological layers are commonly attenuated and boudinaged due to deformation. However, it is difficult to determine whether the lithological layering is a transposed tectonic fabric or whether it reflects a primary volcanic or sedimentary layering because of intense deformation, which occurred during cooling from the metamorphic peak. Therefore, the gross compositional boundaries are referred to as S_1 because they have been significantly modified during deformation and because no evidence for primary bedding or layering has been recognized.

Structural evidence for the earliest deformation(s) has been destroyed by granulite facies recrystallization and anatexis that accompanied peak metamorphism and intense deformation during cooling. Neither F_1 folds nor complex fold interference patterns between later fold generations and F_1 folds have been recognized. An early deformation (D_1) is indicated only by fine-grained inclusion trails in porphyroblasts and a thin gneissosity within discontinuous mafic layers in felsic gneisses. The inclusion trails and thin gneissosity are inferred to represent a tectonic foliation, S_1. Inclusion trails consist of fine-grained sillimanite in granoblastic garnet (Fig. 2.1a) and cordierite in metapelites, and spinel-ilmenite in poikiloblastic garnet (Fig.2.1b) in felsic gneisses. S_1 inclusion trails may also outline isoclinal F_2 folds (Fig. 2.2, Fig. 2.1b). Folded discontinuous

mafic layers and mafic boudins in felsic gneisses may contain an internal foliation defined by mm-scale alternations of two-pyroxene and plagioclase-rich layers, which is correlated with the S_1 inclusion trails in metapelites and garnet-bearing felsic gneisses.

2.22 D_2 deformation

Evidence for the D_2 event is recognized by discontinuous, intrafolial, isoclinal F_2 folds, which fold S_1. Coarse-grained leucosome layers are oriented parallel to the axial planes of F_2 folds and define S_2. Outlines of F_2 folds are defined by S_1 inclusion trails in cordierite and garnet porphyroblasts (Fig. 2.2). An S_1 gneissosity in mafic layers is also folded by intrafolial, rootless isoclinal F_2 folds that are truncated by coarse-grained, cm-scale S_2 leucosome layers. Where unaffected by later deformations, hornblende in the folded mafic layers is aligned parallel to S_2. D_2 deformation also caused boudinage of coarse-grained S_1 garnet within S_2, the garnet layers being folded by F_2 (Fig. 2.1c). Intrafolial rootless F_2 folds are best recognized in felsic gneisses, where they are characterized by extremely attenuated limbs and thickened hinges (Fig. 2.1d). Individual F_2 folds are commonly truncated by leucosome layers defining S_2 (Fig. 2.1e) and by irregular pods and networks of coarse-grained pegmatite. Discontinuous, asymmetrically folded mafic layers and asymmetrical mafic boudins are common in well-foliated felsic gneisses (Fig. 2.1f). Mafic boudins commonly have large separations and their lengths are generally greater than twice their widths. They are flattened parallel to the enclosing S_2 foliation and may contain an internal thin gneissic foliation (S_1) that is folded by F_2. Some more felsic boudins appear to have been partially resorbed, by enclosing leucosomes, probably due to anatexis during deformation. Macroscopic F_2 folds are not common but, in places, are observed to form fold interference patterns with subsequent folds. F_2 fold axes are difficult to measure and an L_2 mineral-elongation lineation is rare, due to the intensity of later recrystallization. However, lineated plagioclase that occurs in some coarse-grained S_2 leucosome layers in felsic gneisses may define an L_2 lineation; it has a variable plunge direction between the southeast and the northeast. Although mesoscopic fold interference patterns indicate that F_2 axes are generally parallel

Fig. 2.1 D_1 and D_2 structures in the Ongeva granulites

2.1 (a) Fine-grained S_1 sillimanite inclusion trails in a garnet porphyroblast from a metapelitic gneiss. Base of photo is 4.4 mm.

2.1 (b) Spinel-ilmenite S_1 inclusions in a garnet porphyroblast from a felsic gneiss. Note the possible outlines of F_2 folds Base of photo is 4.4 mm.

2.1 (c) Elongate garnet defining S_2. Garnet is boudinaged and isoclinally folded (F_2).

2.1 (d) Intrafolial F_2 fold with extremely attenuated limbs and thickened hinge.

2.1.(e) Intrafolial, discontinuous F_2 fold in a well-foliated felsic gneiss. Note late-D_2 pegmatite cutting S_2.

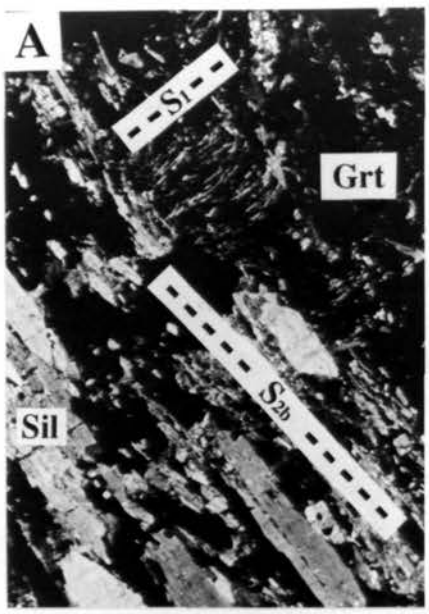
A
S1
Grt
S2b
Sil


B
S1


C
S2

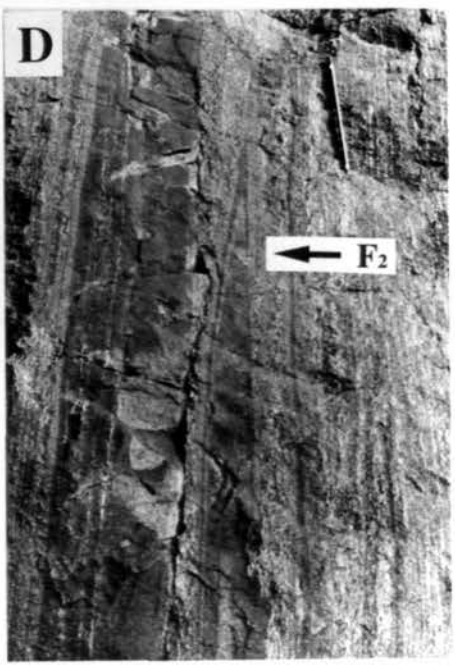
D
F2

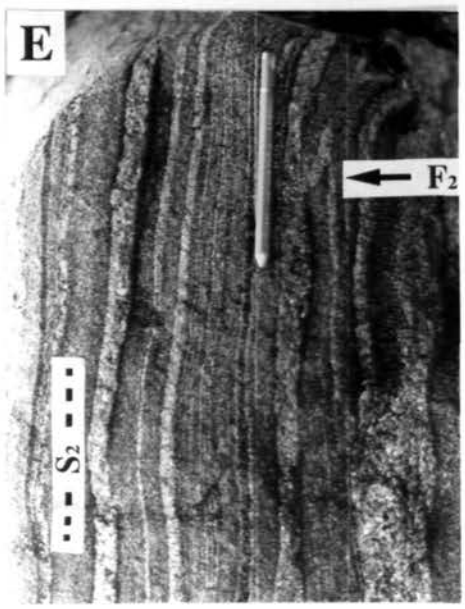
E
F2
S2

Fig. 2.1 (cont'd) D_1 and D_2 structures in the Ongeva granulites

2.1 (f) Asymmetrical mafic granofels boudins and discontinuous asymmetrical F_2 fold with quartz-K-feldspar leucosome defining an-axial plane S_2 foliation.

2.1 (g) Boudins of coarse-grained K-feldspar in S_2 leucosome. Possibly derived from D_1 pegmatite.

2.1 (h) Coarse-grained S_{2b} sillimanite foliation cutting S_2 quartz-feldspar-biotite leucosome.

2.1 (i) Late-D_2, coarse-grained garnet-quartz-K-feldspar pegmatite.

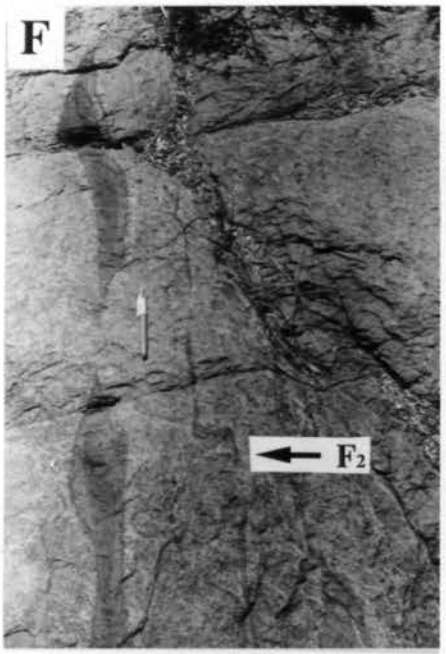
F
F2

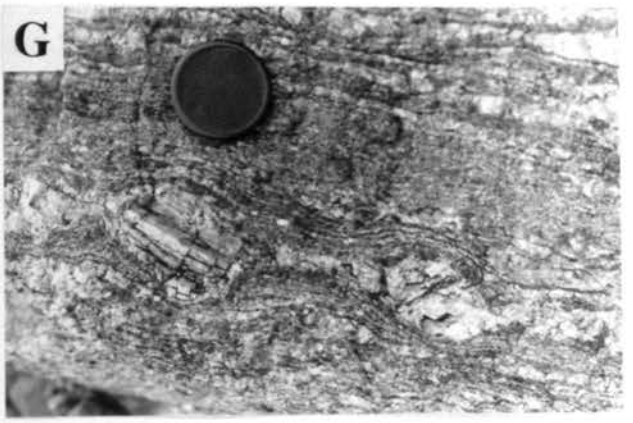
G

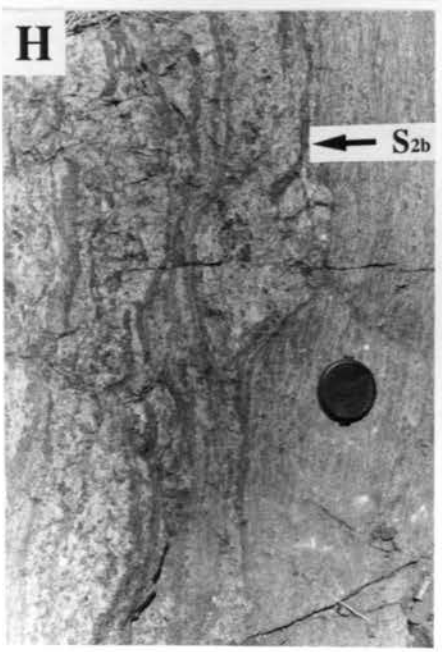
H
S2b

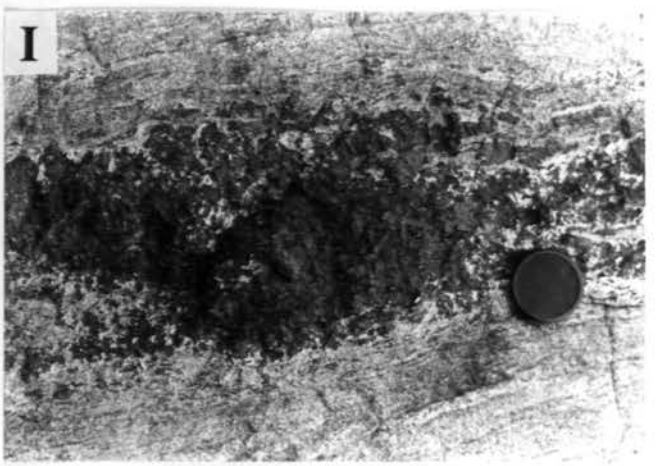
I

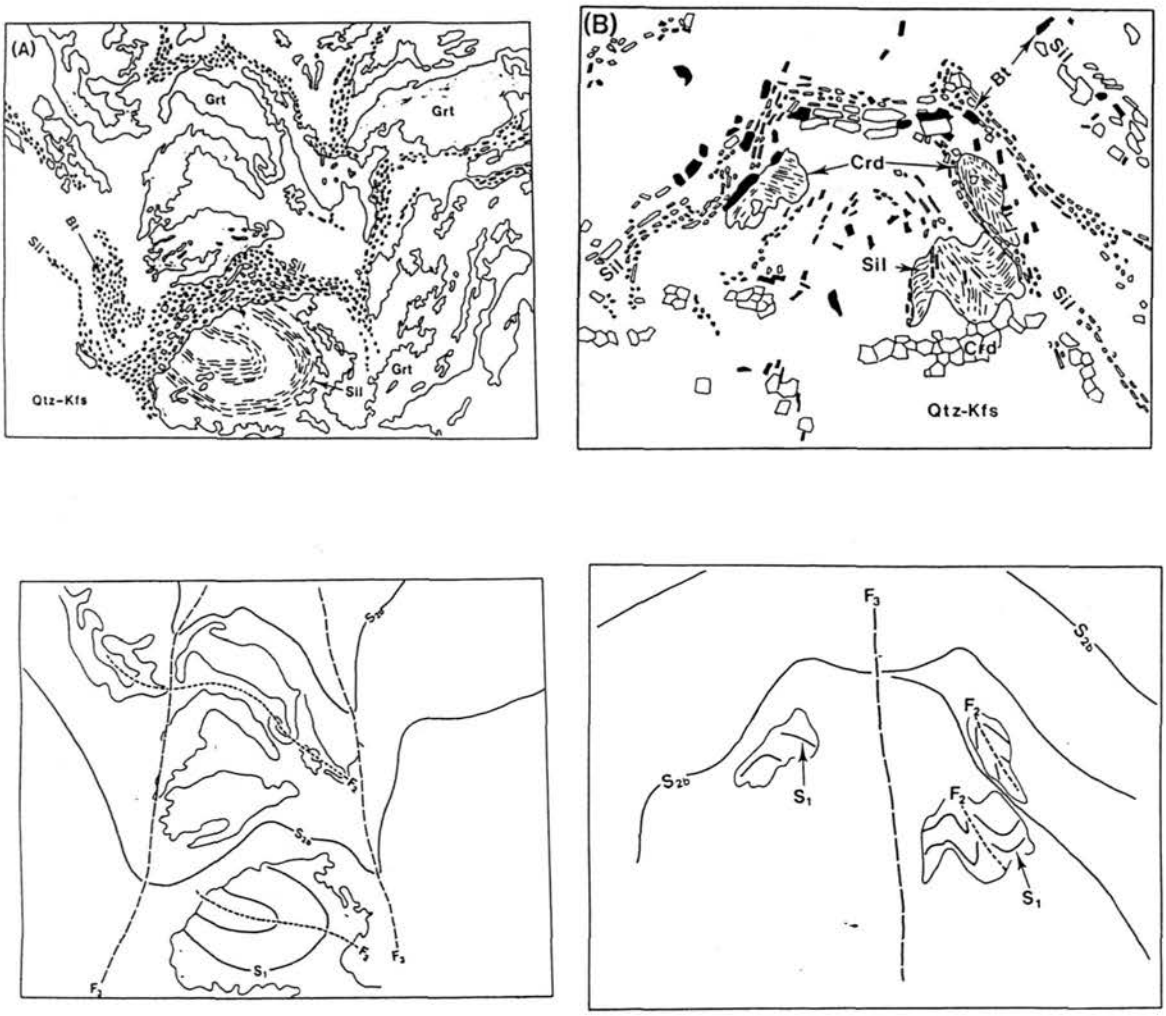

Fig. 2.2 (a) Fine-grained S_1 sillimanite inclusion trails outlining F_2 folds in a garnet porphyroblast from a garnet gneiss deformed by F_3 folds. Sample 766, Ongeva granulites.

2.2 (b) Fine-grained S_1 sillimanite inclusion trails outlining F_2 folds in cordierite porphyroblasts form a metapelitic gneiss deformed by F_3 folds. Sample 823, Ongeva granulites.

to subsequent fold axes, it is difficult to determine whether F_2 axes have passively rotated during subsequent deformation or are in their original orientation.

D_2 predates the deformation(s) responsible for the complex, dominant macroscopic fold pattern in the Strangways Metamorphic Complex and was probably synchronous with the development of the penetrative high-grade gneissic foliation that is developed in throughout the Strangways Metamorphic Complex. This gneissic foliation (S_2) is defined by cm-scale (< 5 cm) variations in mineral proportions, which are distinct from the macroscopic compositional layering. In felsic gneisses, S_2 is defined by medium to coarse-grained quartz-plagioclase±orthopyroxene±garnet leucosome layers (Fig. 1.3a). In metapelitic gneisses, S_2 is defined by medium-grained quartz-K-feldspar±cordierite±garnet leucosome layers (see Fig. 3.1c) and in mafic gneisses, S_2 is defined by plagioclase-rich leucosomes may also contain isolated, coarse-grained orthopyroxene and hornblende (Fig. 2.3). These S_2 leucosome layers are inferred to have formed from the crystallization of partial melt during cooling after the metamorphic peak. In felsic gneisses, very coarse-grained subhedral K-feldspar and plagioclase may be boudinaged and enveloped by medium- to coarse-grained S_2 leucosome (Fig. 2.1g), and may represent residual D_1 pegmatite. S_2 is mostly subparallel to the gross compositional layering (S_1), but locally may be slightly oblique. The angle between S_2 and lithological boundaries is less than 15°. The formation of a layer-parallel leucosome foliation during deformation is discussed later in this Chapter.

Mafic dykes cut the S_2 gneissic foliation and are intensely deformed by subsequent folds. These mafic dykes contain granulite facies assemblages, the mineral compositions of which are similar to those of interlayered mafic gneisses and granofelses in the Ongeva granulites. The mafic dykes do not contain any residual igneous textures. Recrystallized grain boundaries and symplectites that have been attributed to the effects of a second metamorphism (M_2, Chapters 3 and 4) also occur in the mafic dykes. Rare charnockite layers may also be discordant to S_2. A charnockite outcrop that is shown as

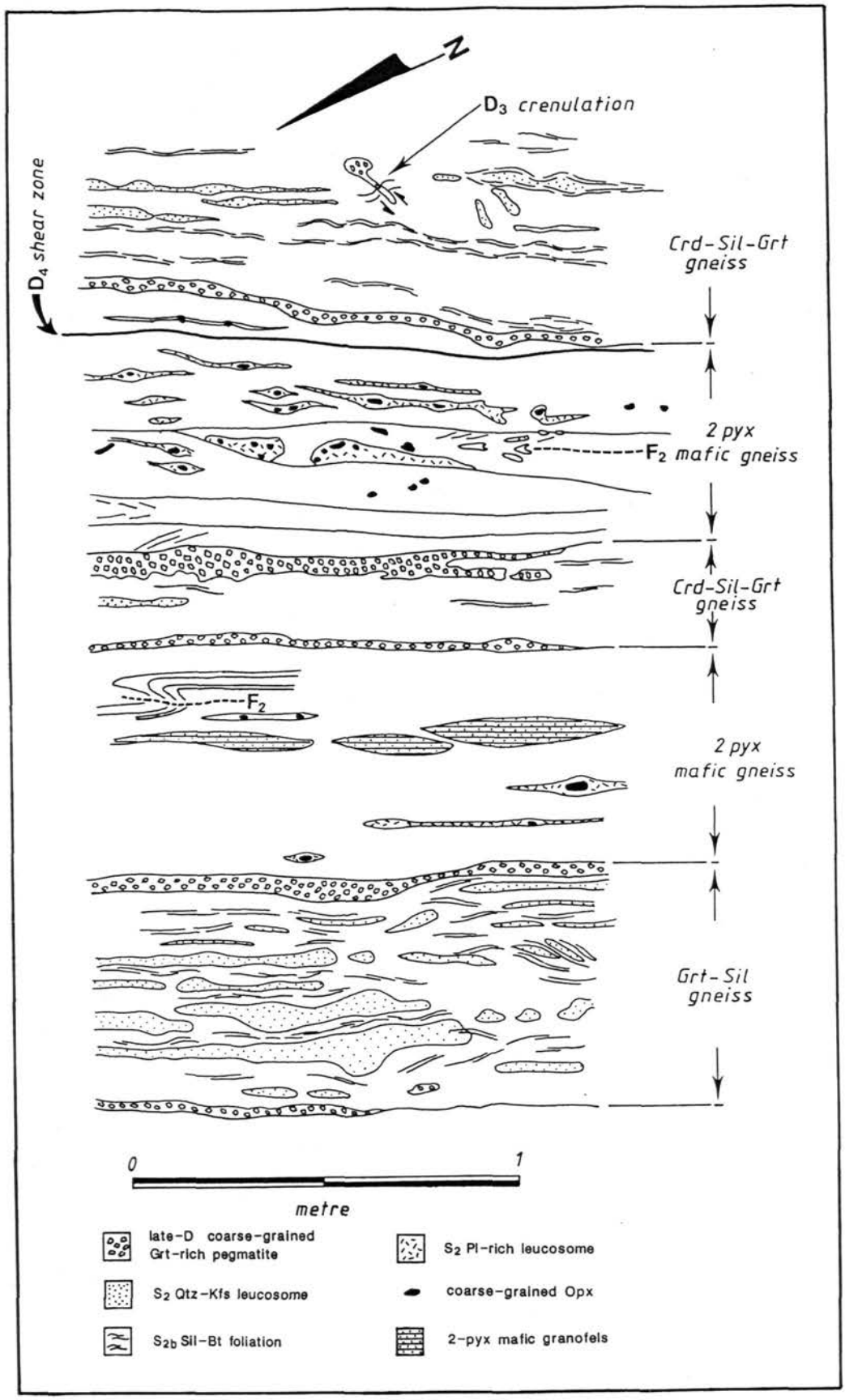

Fig. 2.3 Outcrop sketch showing the accumulation of late-D_2 garnet-rich pegmatite along S_1 lithological boundaries in the Ongeva granulites.

A on Fig. 2.4 contains K-feldspar megacrysts aligned parallel to S_2 indicating magmatic flow (Paterson et al., 1989), but has been intensely deformed by later folds.

In metapelitic gneisses, a coarse-grained sillimanite-biotite-magnetite foliation cuts and anastomoses through the main penetrative S_2 quartz-K-feldspar-cordierite-garnet leucosome layering (Fig. 2.1h). The sillimanite-biotite foliation is generally sub-parallel to the overall trend of S_2 and the S_1 compositional boundaries, and is here designated as S_{2b}. Because of its general similarity in orientation to the S_2 gneissosity and because S_{2b} is deformed by later F_3 folds, the sillimanite-biotite foliation is referred to as S_{2b} and not S_3. For these reasons, S_{2b} is also inferred to preserve the effects of deformation and metamorphism late in D_2. Sillimanite in S_{2b} is poorly lineated, probably reflecting a change in conditions late in D_2. The formation of biotite and magnetite in this foliation indicates that S_{2b} formed during hydrous, oxidizing conditions.

Networks and pods of coarse-grained pegmatite that varies from garnet-quartz-K-feldspar±biotite pegmatite to othopyroxene-plagioclase pegmatite, commonly cut the S_2 gneissosity, but generally have minerals aligned parallel to S_2. In metapelitic gneisses, clear cross-cutting relationships between S_{2b} and irregularly-shaped, coarse-grained pegmatite pods of garnet-K-feldspar-quartz±biotite (Fig. 2.1i, see Fig. 3.1b) are difficult to determine. However, in most places the irregularly-shaped garnet-rich pods cut S_{2b} and contain biotite oriented parallel to S_2 and S_{2b}. In mafic gneisses, coarse-grained plagioclase-rich networks containing orthopyroxene±hornblende cut S_2 (see Fig. 3.1d). The orthopyroxene in these networks is generally rimmed by steel-blue pargasitic hornblende.

In felsic and metapelitic gneisses, coarse grained pegmatite has also accumulated along S_1 lithological boundaries (Fig. 2.3). The bulk mineral compositions in these cross-cutting pegmatites is generally similar to those of the host rock. These features imply that the pegmatite source was local and that the crystallization probably occurred under hydrostatic stress conditions.

The early structural history of D_2 appears to represent deformation synchronous with the crystallization of partial melts in a pervasive gneissic foliation. The later history of D_2 is characterized by the development of coarse-grained sillimanite-biotite foliations and the crystallization of poorly-confined pegmatite and of pegmatite along lithological boundaries, presumably also from partial melts. Successive mineral assemblages that define S_2 suggest that the terrain experienced either isobaric cooling or limited decompression after peak metamorphism (Chapters 3 and 4). The pegmatites also contain microstructures that are indicative of a second metamorphic event (M_2). These features include recrystallized grain boundaries, grainsize reduction and the rimming of orthopyroxene and hornblende by retrograde mineral assemblages. No mineralogical evidence nor structural evidence suggests that a separate major thermal event may have been responsible for the generation of pegmatite; nor is there any evidence of rapid exhumation after D_1 or D_2, which could be responsible for decompression melting at high temperatures. S_2 leucosome layers and late pegmatite pods and networks are inferred to represent the continual crystallization of melt in response to cooling from peak metamorphism (M_1) as the effects of D_2 waned. However, the intrusion of mafic and charnockite dykes and the formation of a sillimanite S_{2b} foliation during D_2 also indicate that thermally perturbed conditions continued to exist during D_2.

The original orientation of D_2 fabrics and the kinematic history of D_2 are difficult to delineate because the early part of the deformation was accompanied by the crystallization of abundant partial melts oriented in the axial planes of F_2 folds. The mineral fabrics in S_{2b} and poorly-confined pegmatite pods are rarely oriented, which also makes the late-D_2 kinematic history difficult to delineate.

2.23 D_3 folding event

F_3 folds

D_3 structures are abundant and form the dominant macroscopic fold pattern in the Ongeva granulites. Two main fold generations (F_3-F_4) have been recognized. The macroscopic fold pattern in the Ongeva granulites is shown in Fig. 2.4 and structural data are presented on stereographic projections in Fig. 2.5.

Discontinuous, tight to isoclinal folds that deform F_2 (Figs. 2.6a, 2.7), S_2 and S_{2b} foliations, as well as pegmatite pods and networks, are referred to as F_3. Three types of mesoscopic F_3 folds occur (types A, B, C), which are distinguished on the basis of different orientations of axial planes and fold axes. The most common F_3 folds (type A) are northeast-plunging, inclined noncylindrical folds. They have east-dipping axial planes and are best developed in felsic gneisses (Fig. 2.6b). The limbs are attenuated and commonly boudinaged. Type A F_3 folds contain a well-developed quartz stretching lineation (L_3) in S_2 that is oriented parallel to the fold axis. These folds are similar to mylonitic folds in shear zones, which have fold axes oriented parallel to a well-defined mineral elongation that defines the principal extension direction during simple shear (Bell, 1978). The rotation of fold axes towards the mineral lineation implies a high-strain deformation (Bell, 1978); the implications of this are discussed later in this Chapter. Although an axial-plane foliation is generally not well developed, and deformation probably involved simple shear strains (K=1; Flinn, 1962), a foliation (S_3) defined by recrystallized quartz may be aligned in the axial planes of some type A F_3 folds. This implies that some deformation may have involved strains with K>1 and was accommodated by axial symmetrical shortening. Where S_3 exists, L_3 occurs as a pervasive S_2-S_3 intersection lineation.

Some type A F_3 folds are doubly plunging (e.g. Mount Schaber), with the fold axis curved in the axial planes. These folds are not common, but contain a well-developed stretching lineation (L_3)' in S_2 that plunges consistently to the northeast and

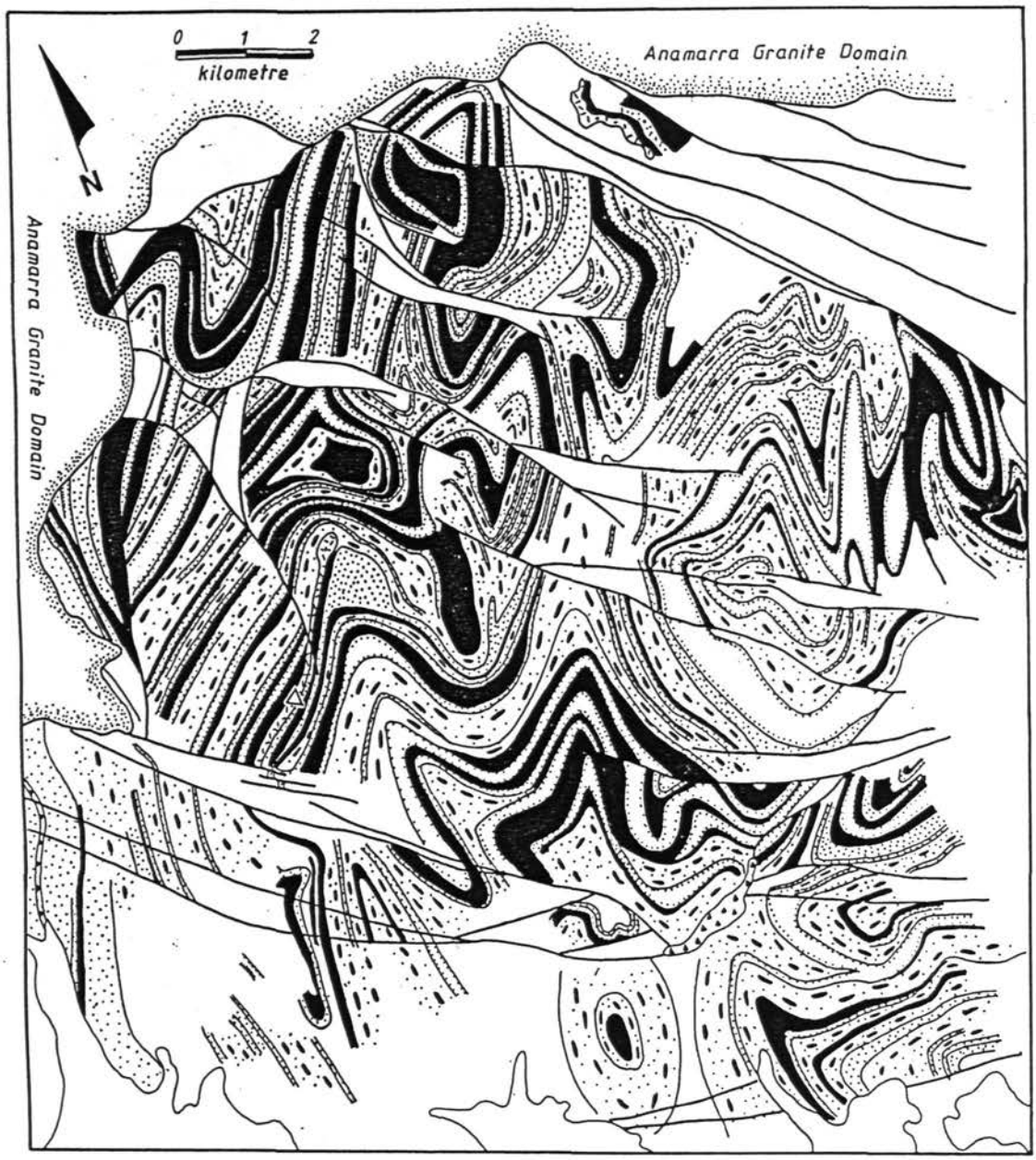

Fig. 2.4 Macroscopic fold pattern in the Ongeva granulites.

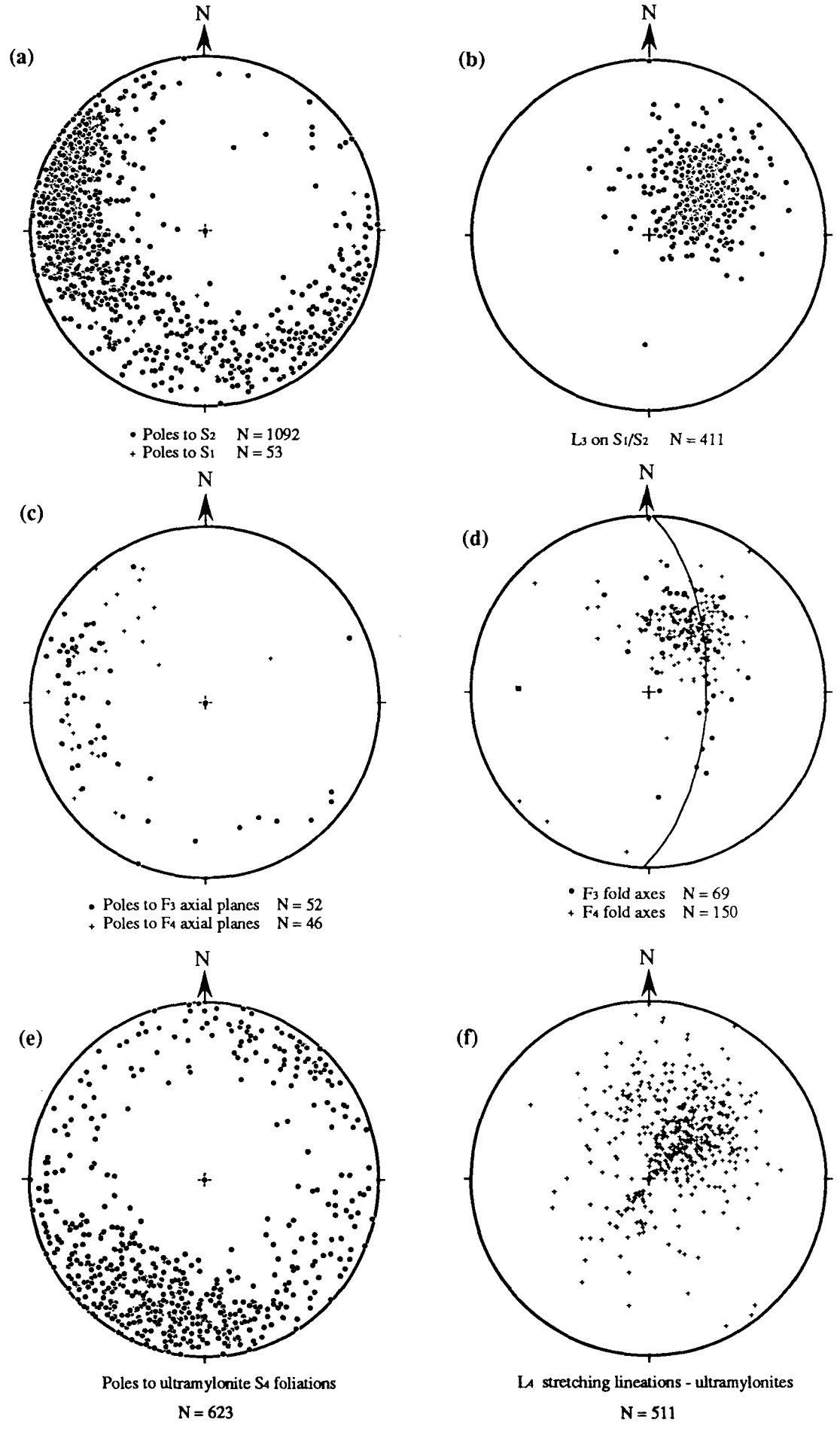

Fig. 2.5 Equal area, lower hemisphere, stereographic projections of structural data from the Ongeva Granulites.

Fig. 2.6 D_3 structures in the Ongeva granulites

2.6 (a) Isoclinal F_2 fold folded by an isoclinal F_3 fold in a felsic gneiss.

2.6 (b) Type A, tight F_3 fold of S_2 leucosome with quartz elongation lineation (L_3) defining a axial-plane fabric (S_3).

2.6 (c) Type B, F_3 fold with quartz elongation lineation parallel to the fold axis. F_3 axial-plane has been reoriented due to F_4.

2.6 (d) Retrograde hornblende and biotite after orthopyroxene defining S_3. S_3 is parallel to the axial-plane of F_3 folds in a felsic gneiss.

2.6.(e) F_3 folded by an open F_4 fold. Note the well-lineated (L_3) coarse-grained late-D_2 pegmatite in top left corner.

2.6 (f) S-shaped parasitic folds on the limb of a macroscopic F_4 fold.

2.6 (g) Garnet-quartz-K-feldspar leucosome segregations parallel to the axial-plane of F_4 folds.

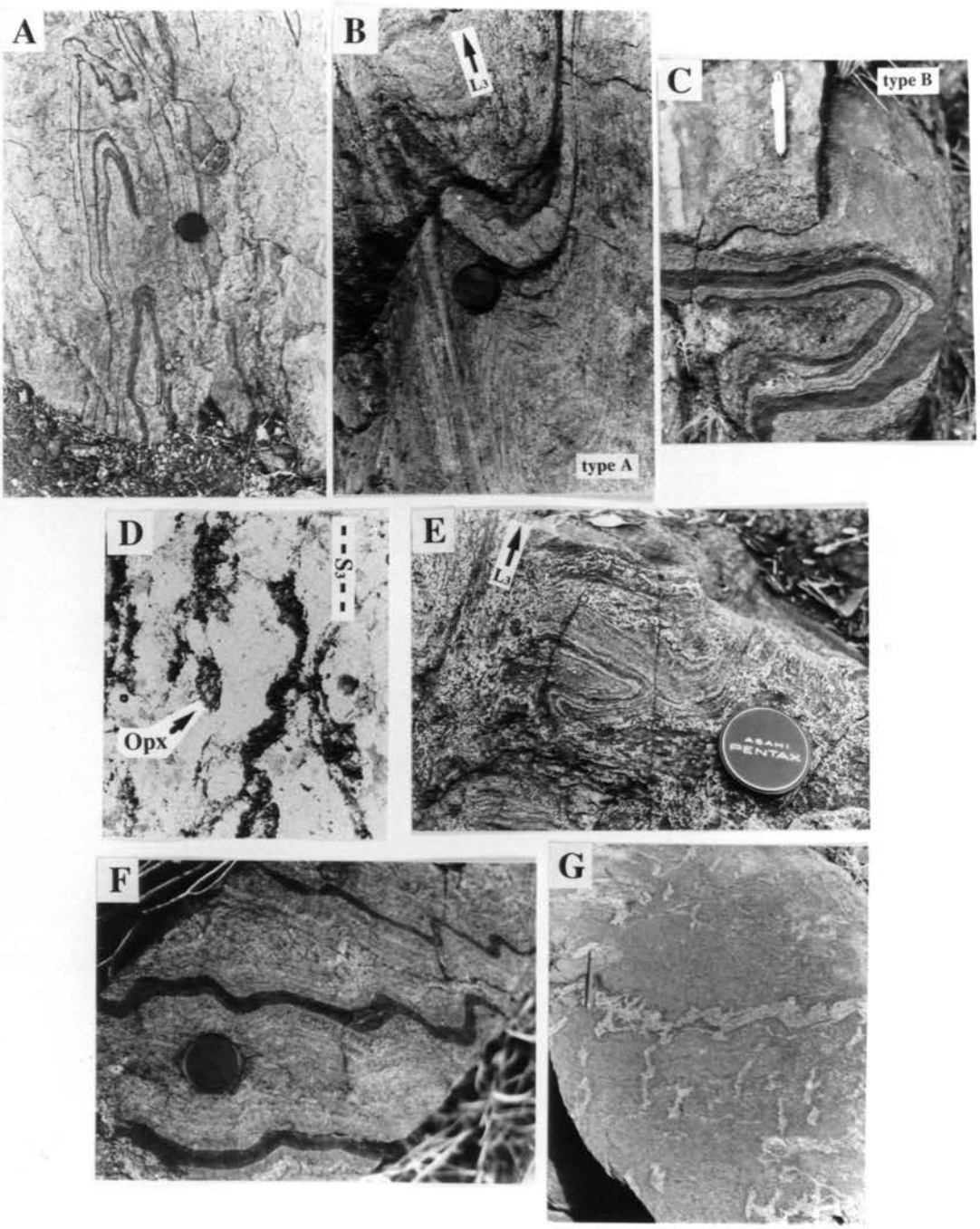
A
B
L3
type A
C
type B
D
Sy
Opx
E
L3
ASAHI
PENTAX
F
G

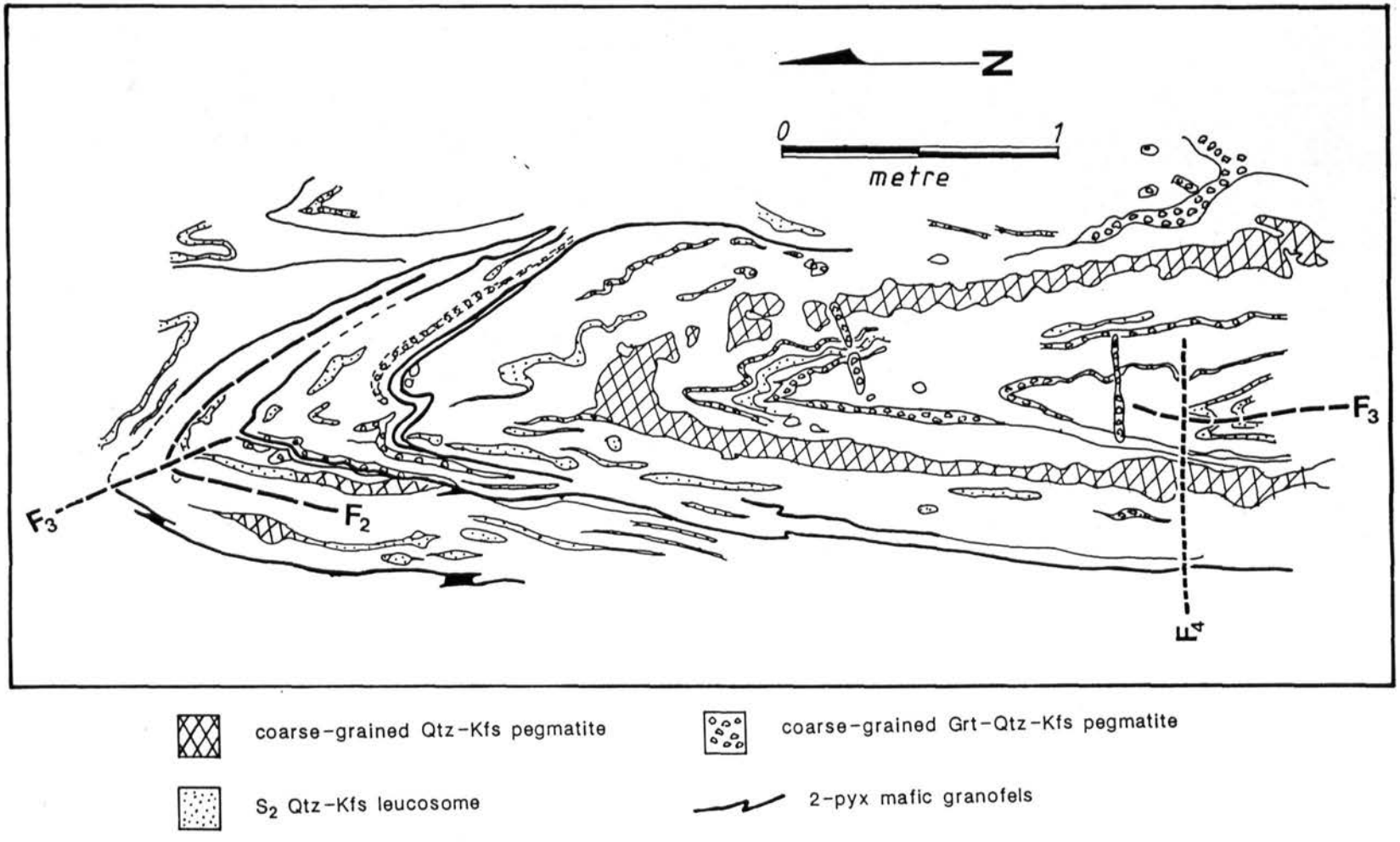

Fig. 2.7 Outcrop sketch of a type-A F_3 in a garnet-bearing felsic gneiss. F_3 folds garnet-bearing S_2 leucosome and F_2 folds. Garnet-bearing pegmatite segregations cut the F_3 axial-plane and are parallel to the axial trace of F_4 folds.

bisects the curved fold axis. Horizontal cross-sections through these doubly plunging folds have flattened shapes, which are parallel to the axial plane. This implies some symmetrical shortening perpendicular to the axial plane. No interference patterns or folding of the stretching lineation were observed, which indicates that the fold patterns were due to refolding. These folds resemble sheath folds, which occur in mylonite zones and in high-strain zones, at the base of nappes and ice sheets (Carreras et al., 1977; Cobbold and Quinquis, 1980; Bell and Hammond, 1984; Skjernaa, 1989) and which also imply high shear strain.

In metapelitic and garnet gneisses F_3 folds may be reclined and contain a mylonitic foliation (S_3) that is oriented parallel to the axial plane. These folds are type B F_3 folds (Fig. 2.6c). The axial plane is generally layer-parallel and is folded by later folds (Fig. 2.8). Type B F_3 folds commonly have east-west trending, north dipping axial planes and northeast plunging fold axes. In orthopyroxene-bearing felsic gneisses, orthopyroxene is rimmed by steel-blue hornblende±biotite, which is aligned parallel to the axial planes of F_3 folds and forms an S_3 foliation (Fig. 2.6d). Grainsize reduction is also observed, with the elongate dimensions of retrograde minerals aligned in the axial planes of type B F_3 folds.

The least common F_3 folds are those with east-west axial planes and subhorizontal fold axes (type C). Type C folds are generally asymmetrical and have a south-directed vergence.

Associated with all F_3 folds is a mineral lineation (L_3), which occurs in S_1/S_2 and S_3. L_3 is defined by elongate quartz or aggregates of garnet and orthopyroxene . L_3 aggregates commonly are five times longer than their widths. L_3 plunges at moderate angles (~50-60°) consistently towards the northeast (051-066).

F_3 folds mostly plunge at about 55 ° to the northeast (032-047; Fig. 2.5d). Minor quartz-K-feldspar-garnet leucosome segregations may be parallel to the axial planes to F_3 folds and coarse-grained pegmatite may occur between boudins on the limbs of type A

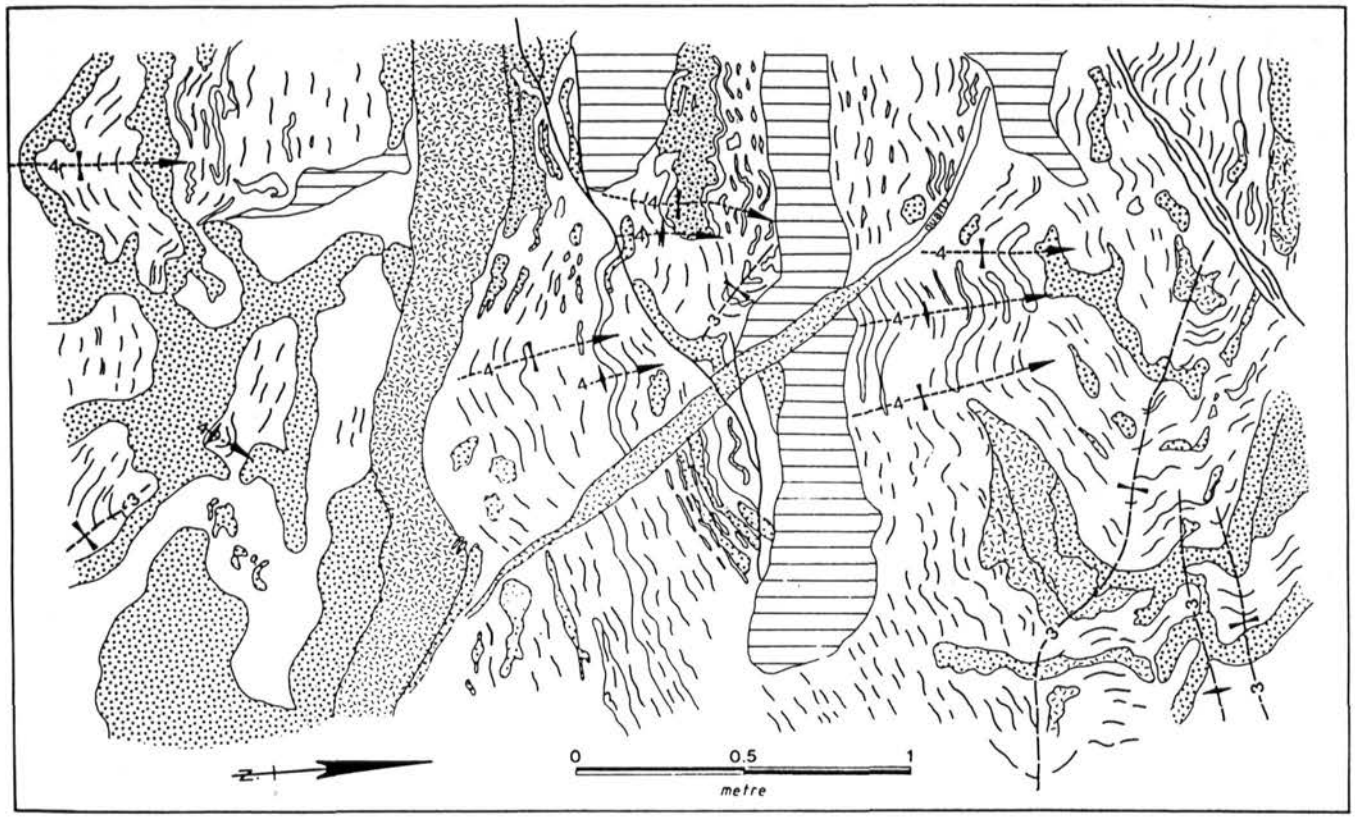

Fig. 2.8 Outcrop sketch of multiply deformed felsic and metapelitic gneisses, showing F_3 and F_4 folds and late-D_2 garnet-bearing pegmatite pods cutting S_2 and S_{2b} foliation. Note that pegmatite dykes cut F_3 and F_4 folds but are displaced by D_4 shear zones.

F_3 folds (Chapter 4, Fig. 4.6). Boudin separation associated with F_3 folds is generally less than the length of the boudin and a lot less than for D_2 boudins. F_3 axial planes are distributed about a small circle with an axis plunging slightly steeper but in the same direction as L_3. The distribution of F_3 axial planes is attributed to subsequent folding (F_4) and the different F_3 fold styles. Although F_3 axes mostly have a northeast plunge, they are distributed about a north-south great circle, which dips 60° to the east. This distribution of F_3 axes is attributed to subsequent deformation (D_4) and is discussed later in this Chapter.

Mafic dykes, which cut the S_2 gneissic foliation, are generally intensely deformed by F_3 folds. However, some mafic dykes also cut F_3 folds but are deformed by subsequent folds (Fig. 2.9), as discussed in the next section.

F_4 folds

Mafic dykes that cut F_3 folds and F_3 axial planes are folded by large, continuous, open, subparallel, plunging, inclined F_4 folds (Figs 2.4, 2.6e, 2.8, 2.9, 2.10). F_4 axes are mostly colinear with F_3 axes, which results in km-scale Type 2 and Type 3 interference patterns (Fig. 2.10; Ramsay, 1967; Thiessen and Means, 1980). The wavelengths of F_4 folds are commonly greater than 2 km. F_4 folds generally have moderate east-dipping axial planes and are commonly asymmetrical with a northwest vergence. Both limbs generally dip to the east, which implies that one limb is overturned. A diagram of isoclinal F_3 folds refolded by open colinear F_4 folds is shown in Fig. 2.11. The enveloping surface of F_4 folds trends southeast and dips to the northeast. Mesoscopic F_4 folds are common, particularly as parasitic folds to large F_4 folds (Fig. 2.6f). F_4 axes plunge mostly at moderate angles (55°) to the northeast (039) and are subparallel to most F_3 axes. No axial-plane foliation was developed in the open F_4 folds, although a poorly-developed quartz elongation lineation is parallel to the F_4 fold axes and sub-parallel to the L_3 stretching lineation. Mesoscopic F_4 folds generally have more parallel styles than F_3 folds, with rounded hinges. Minor quartz-K-feldspar±garnet leucosome segregations are oriented in the axial plane of F_4 folds (Figs.

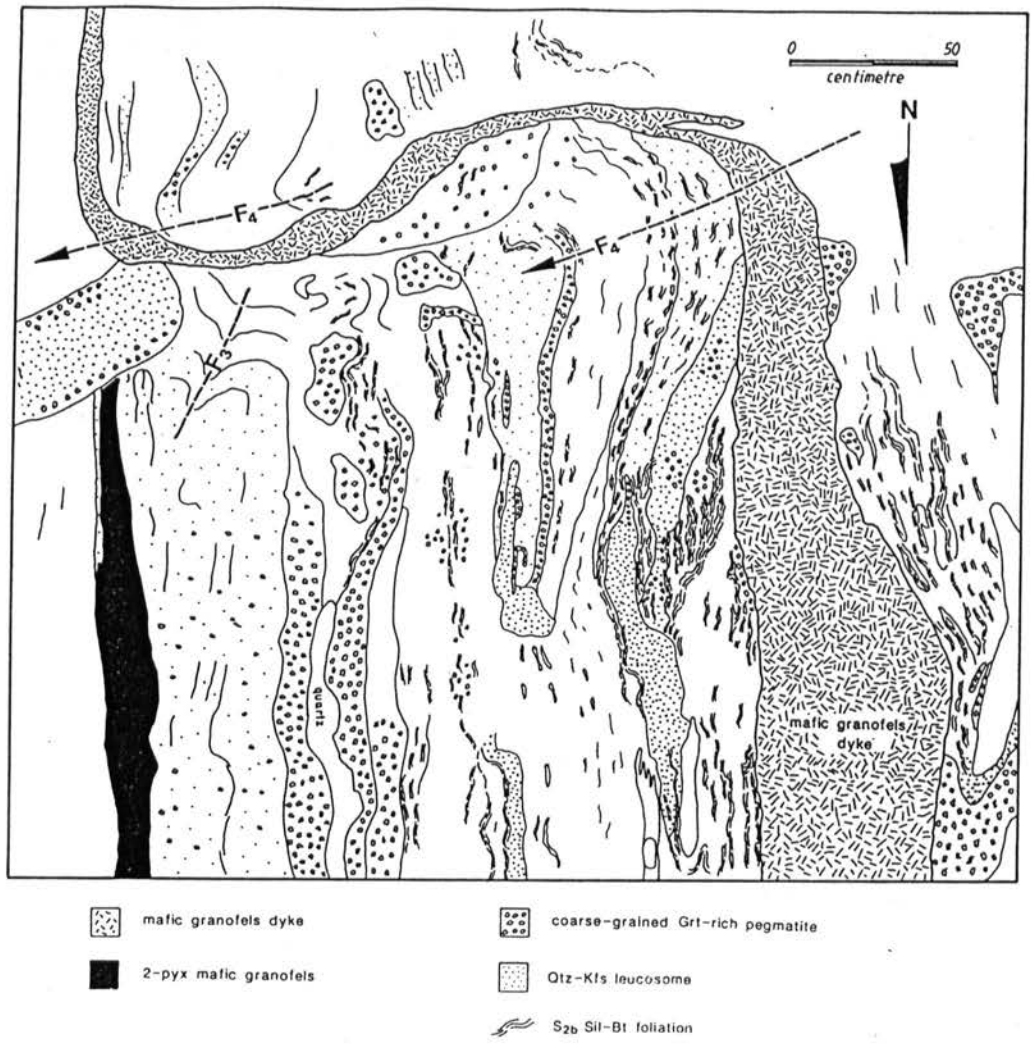

Fig. 2.9 Outcrop sketch of an F_4 folded granulite facies mafic dyke cutting S_2, S_{2b} and F_3 folds.

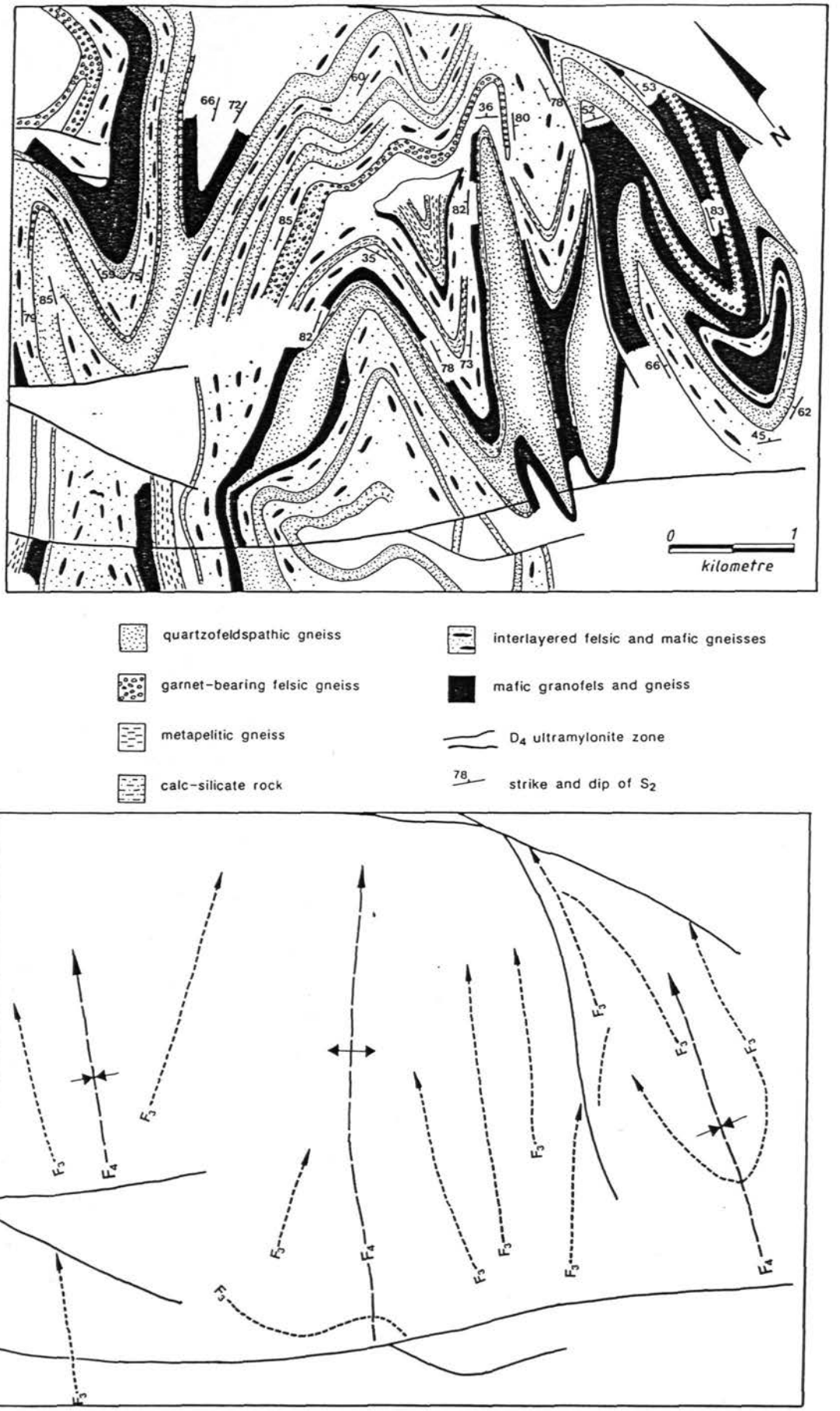

Fig. 2.10 Type 2 and Type 3 (Ramsay, 1967) F_3-F_4 fold interference pattern in the Ongeva granulites.

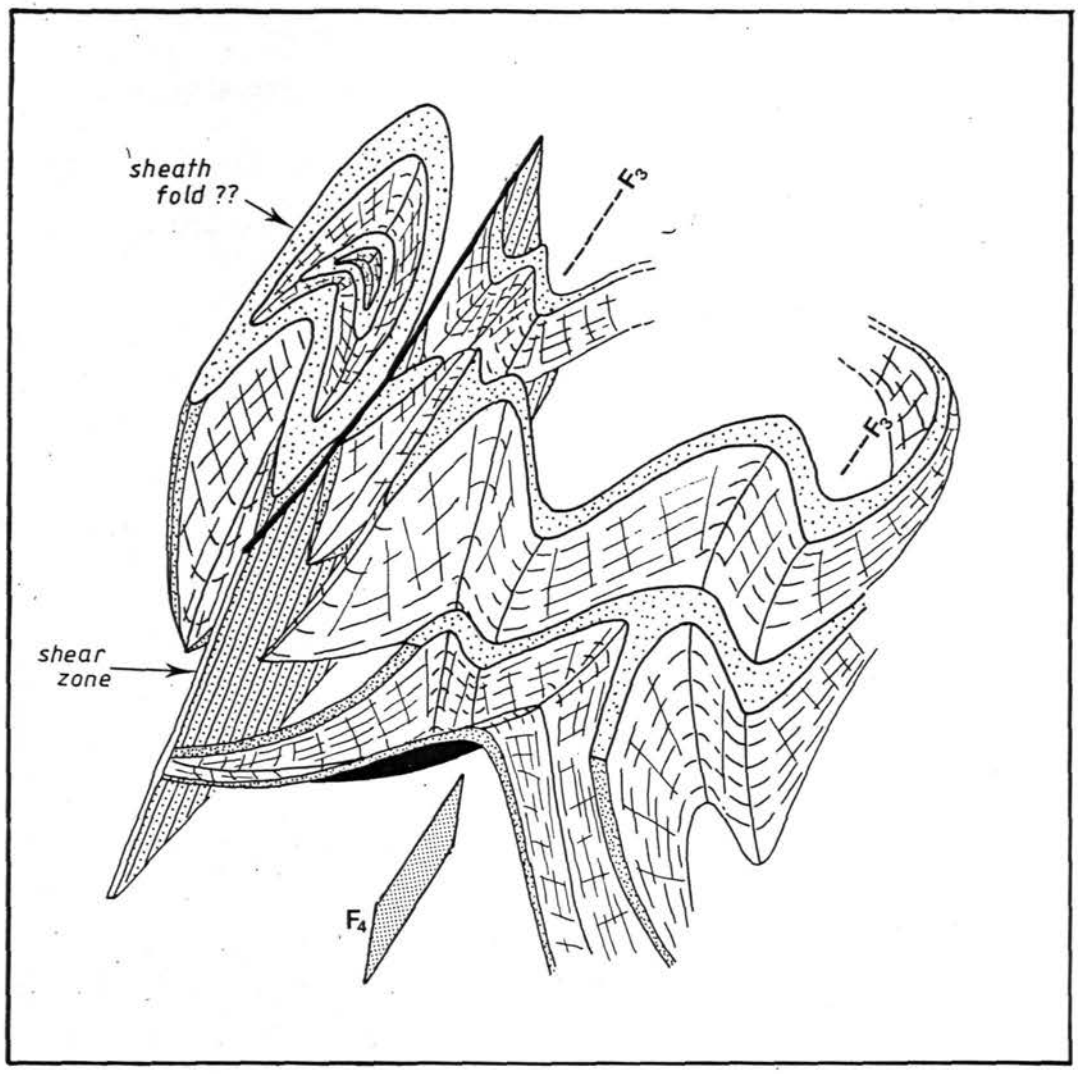

Fig. 2.11 Interpreted 3-dimensional diagram of the fold interference pattern in Fig. 2.10 showing F_3 isoclinal folds folded by more open colinear F_4 folds.

2.6g, 2.7). In places, leucosome segregations occur along conjugate crenulation sets on F_4 limbs (Fig. 2.3), indicating a northeast-southwest shortening direction. These leucosome segregations are inferred to have crystallized from partial melts.

F_3 and F_4 folds have colinear fold axes and are associated with colinear mineral elongation lineations, which suggests that they were the product of a single deformation event that involved simple shear strain accumulations, designated herein as D_3. The noncylindrical, doubly plunging F_3 folds are attributed to heterogeneous deformation during simple shear deformation. The occurrence of pegmatite between F_3 boudins and as leucosome segregations along the axial planes of F_4 folds and crenulation sets, implies that crystallization of leucosome from melt continued throughout D_3. Many F_3 and F_4 folds have inclined axial planes, which may be related to post-D_3 deformation. This is discussed later in this Chapter.

F_4 folds are cut by coarse-grained quartz-K-feldspar-biotite pegmatite dykes. Some contain biotite that defines a foliation parallel to the axial planes of F_4 folds (see Fig. 3.2); they are inferred to be syn-F_4 intrusions. Other pegmatite dykes are undeformed, except by D_4 shear zones (Fig. 2.8) indicating a hiatus between F_4 folding and D_4 shear zone deformation.

2.24 D_4 ultramylonitization

F_3 folds, F_4 folds and pegmatite dykes, which are inferred to represent the effects of progressive deformation during D_3 are cut by discrete shear zones that represent the effects of D_4. These shear zones are characterized by southeast-trending, north-dipping, discontinuous zones of high-grade ultramylonite, which have a consistent north-side down sense of shear (Norman, 1989; Norman and Vernon, 1991; Chapter 5). The shear zones contain a fine-grained mm-scale compositional foliation, S_4. Asymmetrical porphyroclasts commonly occur in S_4 and are good sense of shear indicators (e.g. Passchier and Simpson, 1986). The ultramylonite generally has an internal monoclinic arrangement of mineral fabrics, which is attributed primarily to non-coaxial deformation

(Simpson and Schmid, 1983). Sheath folds are also present. A well-developed lineation (L_4) in S_4 is defined by elongate quartz, and aggregates of garnet and orthopyroxene. L_4 has a steep pitch on S_4 and plunges mostly to northeast along an axis trending 035-215. L_4 is subparallel to D_3 fold axes (Fig. 2.5f). An S_4 foliation may also occur in unmylonitized felsic gneisses parallel to shear zones, and is commonly defined by elongate quartz. There appears to be little displacement of S_1 or S_2 across S_4 in felsic gneisses. However, D_3 fold axes may have been reoriented across S_4. This is discussed later in this Chapter.

The displacement across the shear zones is difficult to determine, due to a lack of marker horizons. A strain analysis was attempted across a rare discontinuous shear zone, which indicated a displacement of 22 m (Chapter 5). The surrounding metamorphic grade preserved in the gneissic rocks does not vary across the shear zones, nor across the Ongeva granulites, which also implies that displacements were small. However, the displacement of lithological units, including the Anamarra granite domain, across prominent shear zones may imply that lateral dextral shear may have occurred prior to dip-slip movement (Chapter 5). D_4 shear zones contain mineral assemblages indicative of granulite facies conditions, similar to those produced during a second metamorphic event, M_2 (Norman 1989; Norman and Vernon, 1991; Chapter 5).

Although the shear zones generally displace F_3 and F_4 folds, some zones follow the folded outcrop pattern (labelled A and B on Fig. 5.1). Both these zones contain a well-defined lineation (L_4) that plunges consistently to the northeast and is not folded. The shear zone labelled A in Fig. 5.1 differs from most shear zones because it preserves well-developed fabrics indicative of reverse movement. The anomalous reverse sense of movement and apparent folded outcrop pattern may imply that strain was partitioned into narrow south-directed zones during the progressive development of F_4 folds. However, reverse shear zones are not deformed by normal zones and lineations in ultramylonite zones throughout the Ongeva granulites are consistently oriented parallel to D_3 fold axes. A plot of ultramylonitic foliations has the same distribution about a northeast-plunging

small circle as S_1 and S_2 (Figs 2.5a and 2.5e). The similar distribution of structural elements in D_4 zones with D_3 structural elements implies that D_3 and D_4 were part of the same deformation cycle.

2.25 D_5 deformation

North of Mount Schaber (Fig.1.1), S_1, S_2, D_3 and D_4 structures in the Ongeva granulites are cut by a north-dipping biotite foliation (S_5). This foliation forms a pervasive structure in the southeast-trending Gough Dam Schist Zone (Fig. 1.1) and is attributed to deformation during D_5. Structural data from the Gough Dam Schist Zone are plotted on stereographic projections in Fig. 2.12. Residual pods of less-deformed gneisses up to 500 m in diameter occur in the Gough Dam Schist Zone. These pods contain a northeast-trending, east-dipping gneissic foliation that is similar in orientation to S_2 in gneisses from the Ongeva granulites, which are undeformed by D_5. This gneissic foliation is folded by F_3 and contains microstructures, such as symplectites, which are attributed to M_2 (Chapter 3 and 4). An F_3 folded cordierite gneiss, within the Gough Dam Schist Zone, that contains M_2 microstructures is shown in Fig. 1.2.

In many places the Gough Dam Schist Zone comprises north-dipping augen gneiss and phyllonite. The original S_2 gneissic foliation has been reoriented parallel to the phyllonitic and biotite foliation. Quartz rodding and a biotite alignment in S_5 define an L_5 lineation. L_5 plunges mostly about 55° to the northnortheast (021), but also plunges towards the northwest and northeast due to later deformation. The plunge direction of L_5 is generally more to the north than L_4 and D_3 fold axes. The distribution of S_5 is like that of S_4. Intrafolial asymmetrical folds, asymmetrical augen and rare oblique shear foliations indicate a south-directed sense of shear. However, most augen in the Gough Dam Schist Zone are symmetrical with respect to the biotite foliation. This suggests that deformation in the Gough Dam Schist Zone may not have been dominated by simple shear. The common orthorhombic symmetry of structures implies a significant pure shear component to the deformation.

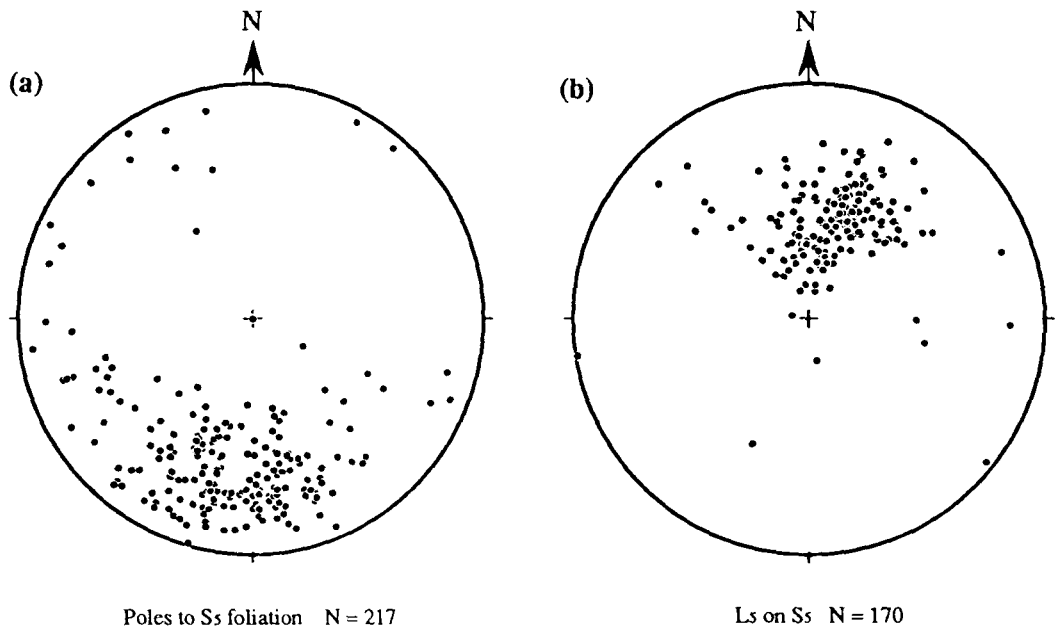

Fig. 2.12 Equal area, lower hemisphere, stereographic projections of structural data from the Gough Dam Schist Zone.

S_5 is folded by near-vertical open folds, which have steep axial planes. These folds resemble conjugate crenulations, with a northwest-trending sinistral set and a northeast-trending dextral set. The distribution in orientation of S_5 and L_5 is probably due to deformation associated with crenulation. The orientation of the crenulation sets indicates an east-west shortening during this later deformation.

A coarse-grained biotite foliation commonly anastomoses through the augen gneiss and the phyllonitic foliation. Biotite in this foliation is elongate parallel to L_5. In places, the foliation is crenulated. A northwest to northeast crenulation cleavage may be developed. Chlorite foliations cut the biotite foliations in the Gough Dam Schist Zone and commonly contain an oblique or subhorizontal mineral elongation lineation. Deformation associated with crenulation and greenschist facies foliations postdated D_5.

2.3 Anamarra granite domain

The Anamarra granite domain (Fig. 1.1) is distinguished from the Ongeva granulites by comprising blocks of deformed megacrystic granite, orthogneisses, metagabbro and layered gneisses that are dissected by continuous mylonitic fabrics. The geology of the Anamarra granite domain is shown in Fig. 2.13 and structural data are presented in Fig. 2.14. The mesoscopic layering and outcrop pattern of orthogneisses and metagabbros are very irregular and intrusive contacts are common (Fig. 2.15a). The blocks of layered gneisses comprise folded quartzofeldspathic gneisses, mafic granofelses and minor cordierite gneisses, similar to gneisses in the Ongeva granulites. In places, layers of granite containing K-feldspar megacrysts are discordant to the layered gneisses. Megacrystic granite does not occur in the Ongeva granulites to the east. Due to extensive dissection by mylonitic foliations, macroscopic fold patterns are rare in the Anamarra granite domain, but three mesoscopic folding phases similar to F_2-F_4 in the Ongeva granulites can be recognized in metapelitic gneisses.

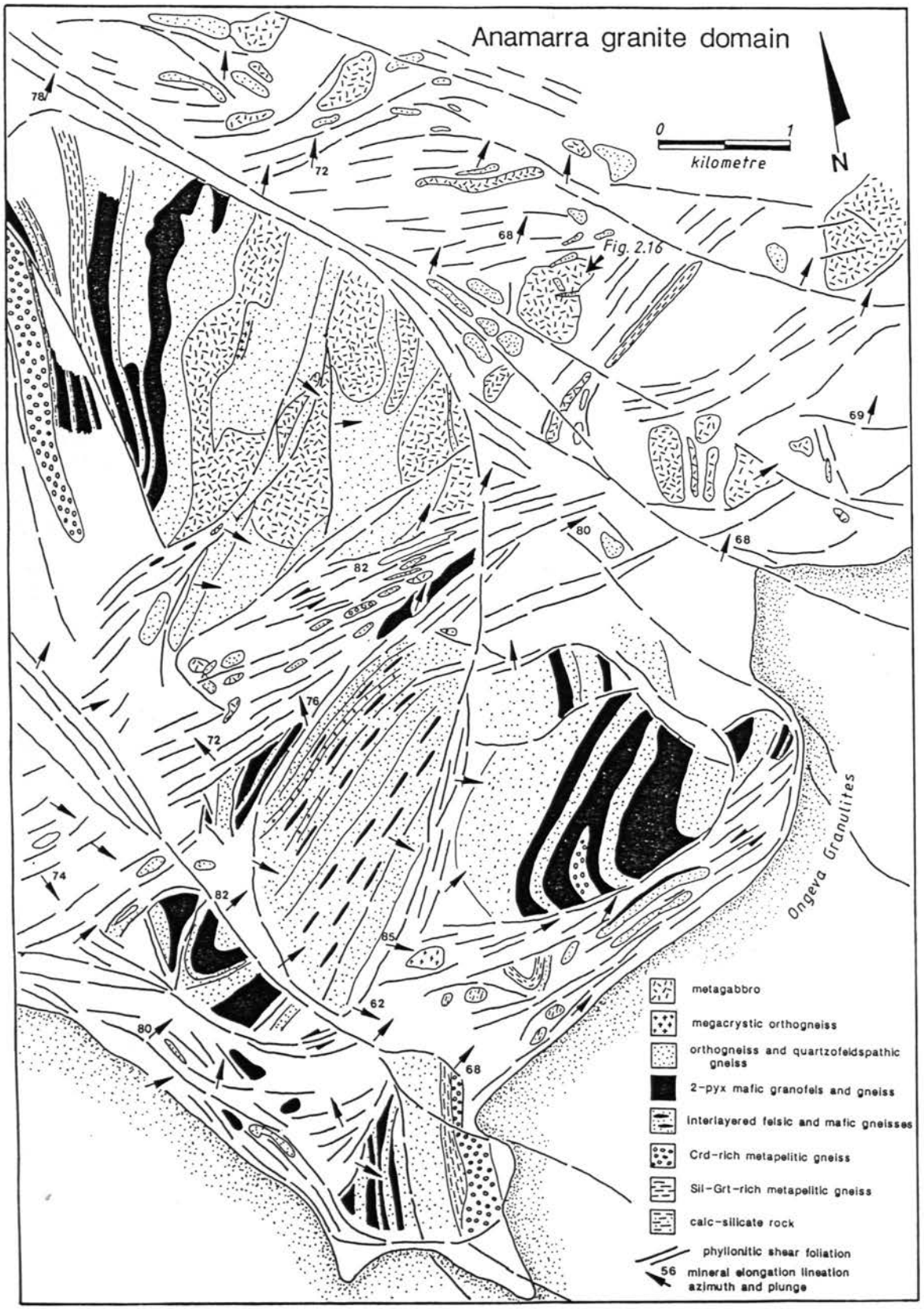

Fig. 2.13 Geology of the Anamarra granite domain.

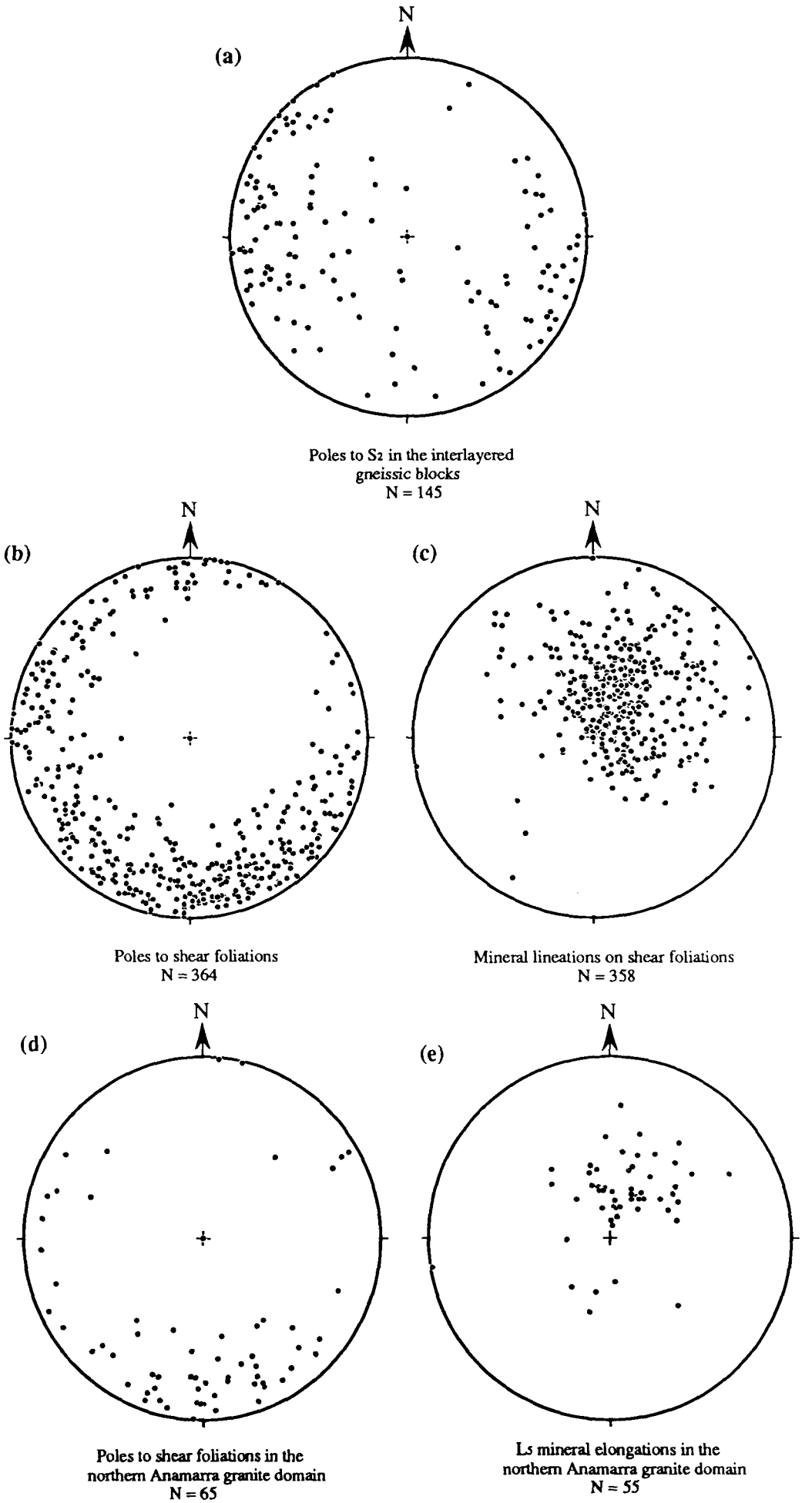

Fig. 2.14 Equal area, lower hemisphere, stereographic projections of structural data from the Anamarra granite domain.

Fig. 2.15 Anamarra granite domain

2.15 (a) Irregular outcrop of orthogneiss and metagabbro in the Anamarra granite domain.

2.15 (b) Elongate cordierite defining S_2. Cordierite is boudinaged and isoclinally folded (F_2).

2.15 (c) Phenocrystic metagabbro enclave in a deformed orthogneiss.

2.15 (d) North-trending shear foliation with asymmetrical folds indicating a sinistral shear sense.

2.15 (e) Crenulated north-trending shear foliation in an orthogneiss.

2.15 (f) Northeast alignment of megacrysts in the Anamarra granite displaced by an east-trending D_4 shear zone.

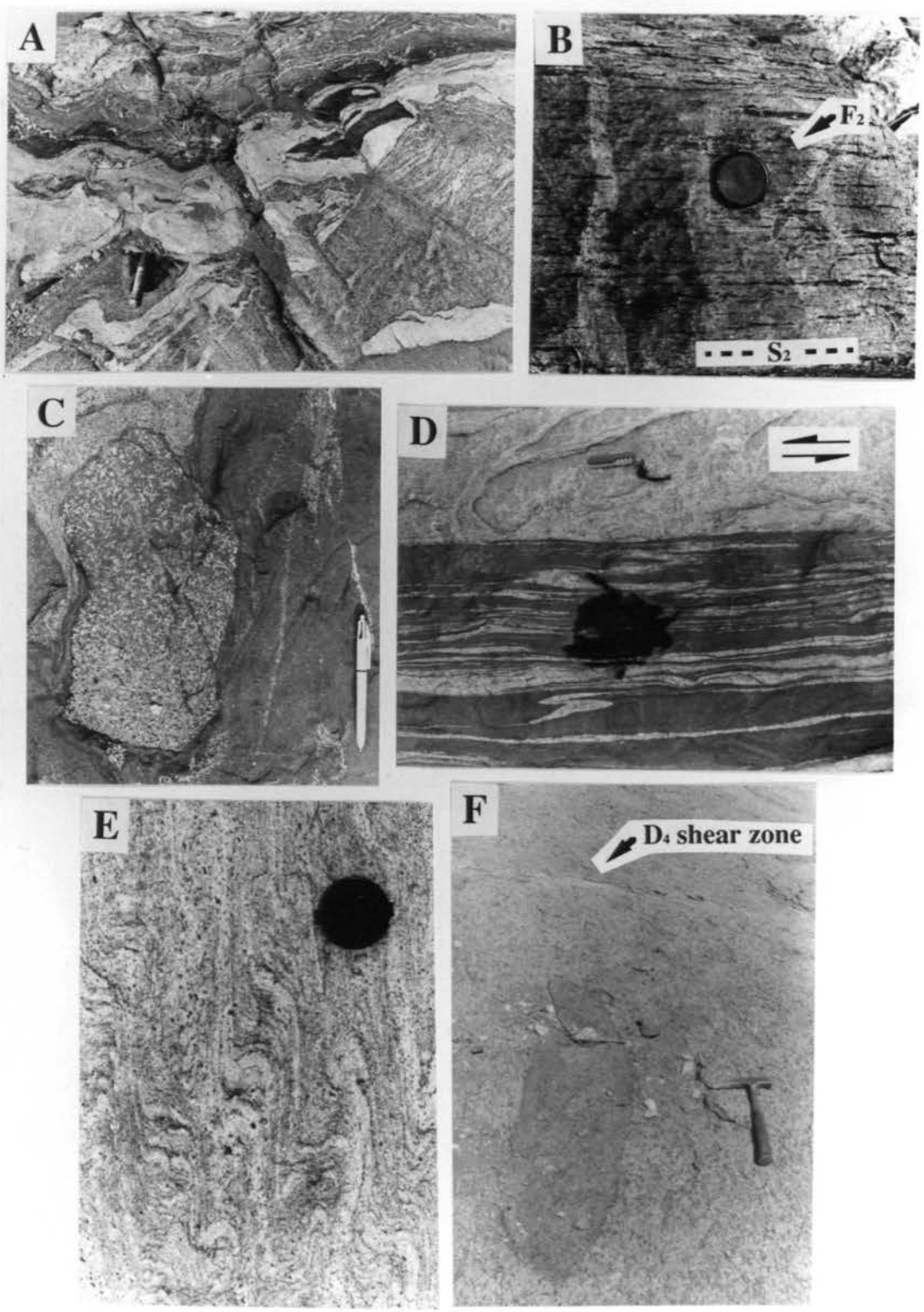
A
B
F2
S2
C
D
E
F
D4 shear zone

2.31 D_1/D_2 deformations

Evidence for the earliest deformations in the Anamarra granite domain occurs in the least mylonitized blocks of layered gneisses. These contain structural fabrics similar to fabrics in the Ongeva granulites. A variation in bulk rock composition also occurs on the cm to m-scale, and massive layers of felsic and mafic granofelses are interlayered with supracrustal rocks. The lithological layers are commonly attenuated and boudinaged due to deformation and the contacts between units are referred to as S_1 (analogous with S_1 in the Ongeva granulites).

Evidence for an S_1 tectonometamorphic foliation has largely been destroyed, due to anatexis and recrystallization during D_2, which produced a pervasive gneissic foliation (S_2). F_1 folds have not been recognized. In cordierite gneisses, a rare S_1 cordierite foliation is boudinaged and isoclinally folded by F_2 (Fig. 2.15b), with quartz-K-feldspar-cordierite leucosomes oriented parallel to the axial planes of the F_2 folds. In felsic gneisses, a gneissosity (S_1) occurs in discontinuous folded mafic layers. Porphyroblast inclusion trails outlining F_2 folds have not been recognized in the Anamarra granite domain.

The earliest folding event is recognized by discontinuous, intrafolial isoclinal folds that occur with coarse-grained leucosome layers (S_2) oriented parallel to their axial planes. These folds are similar to F_2 folds in the Ongeva granulites and have extremely attenuated limbs. The coarse-grained axial-plane leucosome layers are similar to S_2 in the Ongeva granulites. Asymmetrical mafic boudins are also common. Neither macroscopic F_2 folds nor fold interference patterns with subsequent folds have been recognized in the Anamarra granite domain. S_2 trends mostly towards the north and is distributed about a northeast plunging axis (Fig. 2.14a), similar to S_2 in the Ongeva granulites.

In metapelitic gneisses in the Anamarra granite domain, a coarse-grained sillimanite-biotite-magnetite foliation cuts and anastomoses through the main penetrative

S_2 quartz-K-feldspar-cordierite-garnet leucosome layering. This foliation is similar in orientation and composition to S_{2b} in metapelitic gneisses from the Ongeva granulites. Sillimanite in S_{2b} is also poorly lineated in the Anamarra granite domain.

2.32 D_3 folding

Macroscopic D_3 structures are rare in the Anamarra granite domain. A coarse-grained sillimanite-biotite S_{2b} foliation and a S_2 cordierite-bearing leucosome in unmylonitized layered gneisses are folded by tight F_3 folds (see Fig. 3.1c) and more open F_4 folds. Intrusive contacts occur between felsic orthogneisses and layered gneisses, which contain a S_2 foliation. The felsic orthogneisses vary from equigranular quartzofeldspathic gneisses to megacrystic granite and contain inclusions of metagabbro, which may preserve an igneous texture, including large plagioclase laths (Fig. 2.15c). Tight F_3 folds occur in deformed felsic orthogneisses and metagabbro and a typical folded outcrop pattern is shown in Fig. 2.16. The folds are tight to isoclinal and have axes parallel to F_3 and F_4 axes in the Ongeva granulites. The folding of the orthogneisses is attributed to D_3, which produced the macroscopic fold pattern in the Ongeva granulites.

The occurrence of folded leucosome foliations in gneissic rocks and northeast-plunging tight folds suggest that D_3 affected both the Anamarra granite domain and the Ongeva granulites. On the basis of the similarity of metamorphic grade and deformation history, the Anamarra granite domain probably represents a westerly extension of the Ongeva granulites, which was intruded by granite and metagabbro, after cooling from the metamorphic peak. Folded felsic orthogneiss and metagabbro indicate intrusion of the igneous complex syn- or pre-D_3.

2.33 Shear foliations

Two phyllonitic shear foliations occur in zones that enclose the folded gneissic and orthogneissic blocks. They are: (1) a steep northnortheast- to northeast-trending retrograde shear foliation that contains a northeast to southeast-trending biotite elongation

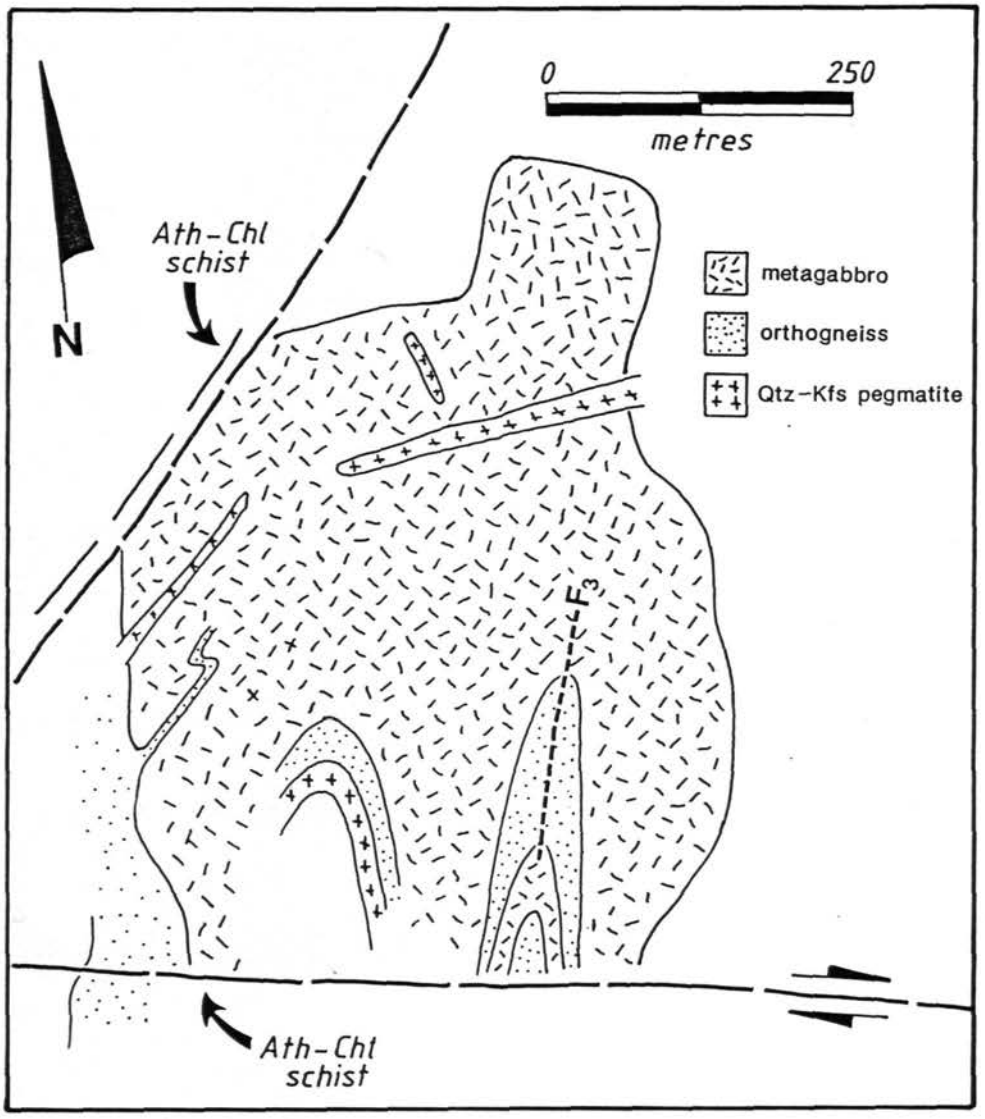

Fig. 2.16 Folded orthogneiss and metagabbro outcrop pattern in the Anamarra granite domain. Location shown on Fig. 2.13.

lineation; and (2) an eastsoutheast-trending shear foliation that contains a northeast trending biotite, quartz or anthophyllite elongation lineation. Both foliations deform irregular networks of phenocrystic felsic orthogneiss and metagabbro. However, the shear foliations in the Anamarra granite domain are commonly further retrogressed, which makes a kinematic analysis of their deformation history difficult. A plot of the structural data from these shear zones is shown in Figs 2.14b and 2.14c.

The north-trending foliation occurs in sub-vertical discontinuous zones up to 100 m wide. The foliation is defined by fine- to medium-grained, cm-scale alternations in mineral composition. These zones generally preserve asymmetrical structures that indicate sinistral shear (Fig. 2.15d). The north-trending foliation bends into and is truncated by the east-trending shear foliation. A lineation is generally not well-defined, but in some felsic gneisses, two lineations may occur. An early steep lineation defined by the preferred orientation of biotite is overprinted by a sub-horizontal lineation defined by a preferred orientation of biotite or anthophyllite. In places, the north-trending foliation is extensively crenulated (Fig. 2.15e) into chevron folds. However, the crenulation is deformed by the east-trending shear fabric.

The north-trending mylonitic foliation in the Anamarra granite domain is deformed by discontinuous zones that contain an east-trending mylonitic foliation. An L-tectonite is commonly well-developed at the intersection of these two shear foliations. The foliation in the east-trending zones is defined by fine-grained alternations in mineral compositions and appears to be continuous with D_4 ultramylonite zones in the Ongeva granulites. The zones dip at moderate angles to the northeast and vary in width from several mm to 100 m. The east-trending foliation cuts F_3 isoclinal folds of felsic orthogneiss. Greenschist facies retrogression commonly occurs along the east-trending shear zones, the extent of retrogression varying within individual zones. Whereas chlorite-bearing greenschist facies assemblages occur in the centre of the zones, metagabbro is retrogressed to anthophyllite-bearing assemblages on the margins of the zones. This suggests that multiple metamorphisms accompanying deformation occurred along the east-trending

shear zones. Biotite schist, which may be extensively crenulated occurs in places. Biotite may be replaced by muscovite. Crenulation of the biotite schist and the retrogression are probably related to post-D_5 deformation.

The largest intrusion in the area is a megacrystic granite called the Anamarra Granite (Shaw and Langworthy, 1984). It contains a sub-horizontal, northeast-trending alignment of megacrysts, which is cross-cut by narrow, discrete, eastsoutheast-trending mylonite zones (Fig. 2.15f). Deformation increases in intensity around the margin of the granite. The alignment of megacrysts in a foliation parallel to the regional northeast-trending shear foliation (D_3?) may suggest that crystallization of the granite occurred during or prior to D_3. The east-trending shear zones, which deform the Anamarra Granite are continuous with other east-trending shear zones in the Anamarra granite domain that appear to be continuous with D_4 ultramylonite zones in the Ongeva granulites. This indicates that intrusion of the Anamarra granite occurred before D_4 and had crystallized sufficiently to accommodate heterogeneous deformation in shear zones. Displacement of the Anamarra granite across the east-trending shear zones is difficult to determine, but appears to be small.

2.34 D_5 deformation

In the northern part of the Anamarra granite domain, both the northnortheast- and east-trending shear foliations contain a well-developed lineation defined by elongate quartz that plunges to the northnortheast. This lineation is colinear with L_5 in the Gough Dam Schist Zone. Asymmetrical folds, asymmetrical augen and oblique shear foliations preserved in an east-trending phyllonitic foliation indicate a north-side-up sense of shear.

Deformation on the northern margin of the Anamarra granite domain is probably due to reworking during D_5. This deformation is correlated with deformation in the Gough Dam Schist Zone, which outcrops to the north of the Anamarra granite domain.

2.4 Structural evolution of the Strangways Metamorphic Complex

The structural evolution of the Strangways Metamorphic Complex may be attributed to two major deformation cycles (D_{1-2} and D_{3-5}). A summary of the structural elements produced during these deformations, age constraints and interpreted deformation styles are shown in Table 2.1. Deformation during the first cycle was accompanied by anatexis induced by peak metamorphism (M_1), with the deformation of leucosome during D_2 indicating that the initial crystallization of partial melt predated D_2. Evidence for D_1 is only preserved by fine-grained inclusion trails and a thin gneissosity in discontinuous mafic layers in felsic gneisses. Effects of D_2 are characterized by asymmetrical folds, asymmetrical boudins and an S_2 leucosome foliation parallel to the axial planes of F_2 folds. Although S_2 commonly is subparallel to the lithological layering, the intensity of recrystallization during D_2 was such that the lithological layering was rotated everywhere into parallelism with S_2. Evidence for such intense deformation is commonly observed in high-grade terrains (e.g. Sandiford, 1989a). There appears to be no large-scale repetition of "stratigraphy" associated with D_2 in the Strangways Metamorphic Complex and successive mineral assemblages indicate that peak metamorphism was followed by near-isobaric cooling or limited decompression (Chapters 3 and 4). This implies that significant crustal thickening did not occur during D_2.

In places, S_2 is slightly oblique to S_1. This obliquity and the common occurrence of asymmetrical structures and large boudin separations in S_2 indicate extreme extension, probably involving large simple shear strain accumulations. However, it is difficult to determine the original orientation of D_2 fabrics and a D_2 tectonic axis, due to the intensity of deformation during D_3 and the dissection of the terrain by later shear zones. U-Pb ion microprobe data obtained from zircons extracted from a intrusive charnockite, which is deformed by D_3 and slightly discordant to the S_1 lithological layering, indicate that D_2 occurred at 1765±4 Ma (Norman and Collins, unpublished data). Peak metamorphism in

Table 2.1 Summary of the structural evolution of the Strangways Metamorphic Complex.

age (Ma)	deformation	structural elements	deformation model
1820-1790	D_1	S_1 inclusion trails S_1 mesosomes	crustal thickening due to magmatic accretion lithospheric extension
1765[A]	D_2	F_2 isoclinal, intrafolial rootless folds S_2 leucosome, layer-parallal foliation mafic dykes	ductile non-coaxial extension
		S_{2b} foliation non-confined partial melt	nil terrain cooled
1745[B]	D_3	F_3 mylonitic folds F_4 open folds mafic dykes	progressive non-coaxial deformation axial symmetric extension crustal thickening
		southeast dextral shear zones northeast sinistral shear zones	mega-scale kink zone northeast-southwest coaxial shortening
	D_4	north-down ultramylonite zones	gravitational collapse or antithetic shearing
	D_5	north-up wide shear zones	non-coaxial thrusting followed by a flattening-style of strain
	post-D_5	conjugate crenulation westerly tilt of terrain	east-west shortening

[A] Intrusion of charnockite. Zircon data (A. R. Norman and W. J. Collins, unpublished data)

[B] Intrusion of the Anamarra granite. Zircon data (A. R. Norman and W. J. Collins, unpublished data)

the Strangways Metamorphic Complex is inferred to have occurred at about 1800 Ma (Black et al., 1983; Windrum and McCulloch, 1986).

Due to the intensity of recrystallization, structures associated with the tectonic history of the Strangways Metamorphic Complex prior to peak metamorphism have been destroyed. However, the metamorphic fabrics comprising the Strangways Metamorphic Complex, which are described above, allow some inferences concerning the possible tectonic settings for D_{1-2} and D_{3-5} to be made. Granulite facies metamorphism involves a gross perturbation of the normal continental geotherm, which requires the existence of a very thin lithosphere and/or an external source of heat. Peak metamorphism in the Strangways Metamorphic Complex accompanied the development of S_1. The heat required for the metamorphism must have been from outside the Strangways Metamorphic Complex, possibly involving a thinned lithosphere. Mafic dykes and charnockite intruded during D_2 suggesting that metamorphic conditions in the Strangways Metamorphic Complex were still thermally perturbed by mantle processes during D_2. Since deformation during D_2 followed peak metamorphism sooner than the time required for thermal relaxation of the continental lithosphere, namely about 60 Ma (England and Richardson, 1977; Loosveld and Etheridge, 1990), the mantle perturbations inferred to have accompanied D_2 could have been a continuation of the processes responsible for peak metamorphism (Chapters 3 and 4). Therefore, D_1 and D_2 probably resulted from one deformation cycle that was responsible for, and a consequence of, granulite facies metamorphism.

In high-grade Proterozoic terrains elsewhere, the high geothermal gradients have been attributed to the intrusion of granites (Oxburgh and Turcotte, 1970; England and Thompson, 1986) and the development of layer-parallel gneissic foliations has been attributed to a number of processes involving crustal thickening or crustal extension (Park, 1981; Bohlen, 1987; Sandiford, 1989a). Sandiford and Wilson (1984) have suggested that magmatic overaccretion was responsible for initiating gravitational instability that resulted in recumbent folds and a high-grade, layer-parallel foliation in the

Napier Complex, Antarctica. Tectonic models have also been proposed for the formation of Proterozoic crust, which involve substantial underplating (Etheridge et al., 1987; Wyborn et al., 1987). In rocks from the Strangways Metamorphic Complex, the only evidence that crustal overthickening may have occurred prior to M_1 is preserved in mineral zoning, which indicates that limited decompression occurred after peak metamorphism (Chapter 4). Although there is little evidence for large-scale magmatic accretion in the Strangways Metamorphic Complex during M_1 or D_2, significant granite and mafic intrusions appear to have occurred elsewhere in the Arunta Block in the period 1760-1820 Ma. In the northern Arunta Block, large megacrystic granitoids that contain zircons dated at 1820 Ma (Collins et al., 1991) intrude Division 1 rocks, belonging to the Lander Rock Beds (Clarke et al., 1990). Numerous other granites and orthogneisses in the northern Arunta Block and adjacent Davenport Province contain zircon populations dated at 1760 Ma (Collins et al., 1991). Rocks surrounding the granitoid intrusion have mineral assemblages indicating low-pressure metamorphism (Clarke et al., 1990; Clarke and Powell, 1991). Teleseismic travel-time residuals across the Arunta Block also suggest that the crust contains a gabbroic underplate (Drummond, 1988). Crustal thickening due to magmatic accretion during D_1/M_1 and D_2 could have created gravitational and isostatic instabilities that resulted in sub-horizontal extension and the formation of a layer-parallel S_2 tectonic foliation: a crust weakened by anatexis could have facilitated extensional deformation.

Cooling of the terrain continued as D_2 waned. Cross-cutting features indicate that late in D_2 the crystallization of unconfined partial melts and local hydration in metapelites occurred to produce a sillimanite-biotite foliation. There is no evidence for any significant uplift after D_2 and conditions remained at granulite facies during slow cooling of the generally dry terrain (Chapter 4).

The D_3 deformation was largely responsible for the complex fold pattern in the Strangways Metamorphic Complex and is part of a deformational cycle unlike that of D_1/D_2. U-Pb ion microprobe data obtained from zircons extracted from the pre- to syn-

D_3 Anamarra granite indicates that D_3 occurred at 1745±4 Ma (Norman and Collins, unpublished data). Deformation during the early part of D_3 was probably homogeneous and involved a significant simple shear component. Finite extension occurred along a northeast plunging axis (~055), which is recognized by the well-developed pervasive stretching lineation (L_3). This is also inferred to be the tectonic transport axis during D_3 (after Shackleton and Ries, 1984). No variation in metamorphic grade has been recognized in this study area, which implies that displacements were small during all the D_1-D_5 deformations and subsequent shear zone deformations. On the basis of the consistent orientation of D_3-D_5 linear structural fabrics, the present orientation of L_3 and D_3 fold axes is probably similar to their initial attitude. Colinear folding of F_3 folds produced large northeast-plunging F_4 folds. Incipient (?) partial melt crystallized between F_3 boudins and in the axial planes of F_3 and F_4 folds. Conjugate shears on the limbs of F_4 folds also indicate that northeast-southwest coaxial shortening occurred during the later part of D_3. D_3 fold axes plunge mostly to the northeast (~035), which is about 20° to the north of L_3. There is also a spread of axes towards the north, which may be attributed to the rotation of fold axes during D_3 towards the finite extension direction during progressive shear. This is inferred to have occurred during deformation dominated by simple shear (Bell, 1978). The distribution of D_3 axes indicates that rotation of the fold axes occurred in a clockwise direction. Some F_3 and F_4 folds are asymmetrical and have an east to west vergence. Most axial planes also dip to the east. This asymmetry also indicates a northeast to southwest transport direction provided the fold styles are original D_3 structures.

Assuming that the the Anamarra granite domain and the Ongeva granulites were once contiguous, the position of Anamarra granite domain, north of the Ongeva granulites, can be explained by lateral dextral shear along the Cadney Fault (see Fig. 5.1). However, this shear zone preserves a steep lineation (L_4) and evidence for a normal sense of movement. Steep normal movement is inferred to have overprinted lateral dextral shear. The mineral fabrics comprising other prominent shear zones (e.g. the Mount Johnstone Fault) also preserve a normal sense of movement, but appear to have involved

dextral shear, on the basis of offsets of major lithological units. Dextral shearing occurred before D_4 and probably after D_3 folding, and may have been associated with the development of a north-trending sinistral shear foliation in the Anamarra granite domain. The dextral zones dip to the north and are discrete. The sinistral zones are steep, contain both steep and subhorizontal lineations, and are more closely spaced and continuous than the dextral zones. The sinistral and dextral zones may form part of a large kink zone, produced during axial symmetrical shortening along an axis trending parallel to L_3, late in D_3 (Fig. 2.17). A northeast-trending anisotropy consisting of L_3 and S_2 would have assisted in producing a large-scale kink zone. Rotation of D_3 axial planes, which resulted in their their common easterly dip, may also have occurred between the dextral shear zones. The north-dipping enveloping surface of D_3 folds and an inferred subhorizontal shortening during kink zone formation imply that D_3 occurred during compression of the Strangways Metamorphic Complex.

D_4 deformation is characterized by steep north-dipping ultramylonite zones that preserve a normal sense of movement. Deformation occurred at granulite facies conditions. Shear zone stretching lineations occur in the enveloping surface of D_3 folds and plunge along an axis that is parallel to D_3 fold axes. There appears to be little displacement across the D_4 shear zones. However, a north-south great-circle distribution of some F_3 axes may imply that limited shear-related folding of D_3 folds and shortening between the shear zones has occurred. The easterly dip of this great circle distribution could also reflect a broad westerly tilt of the terrain. D_4 represents either crustal collapse after D_3 compression or antithetic shear zones developed between larger shear zones with reverse movement. The colinearity of fabrics during D_3 and D_4 suggests that they are part of the same deformation cycle.

The effects of D_5 deformation are concentrated in wide zones consisting of phyllonite and augen gneiss. These zones preserve evidence for south-directed shearing. Lineated sillimanite in these zones indicates that deformation initially occurred in the sillimanite stability field. Mineral lineations (L_5) in these zones plunge to the

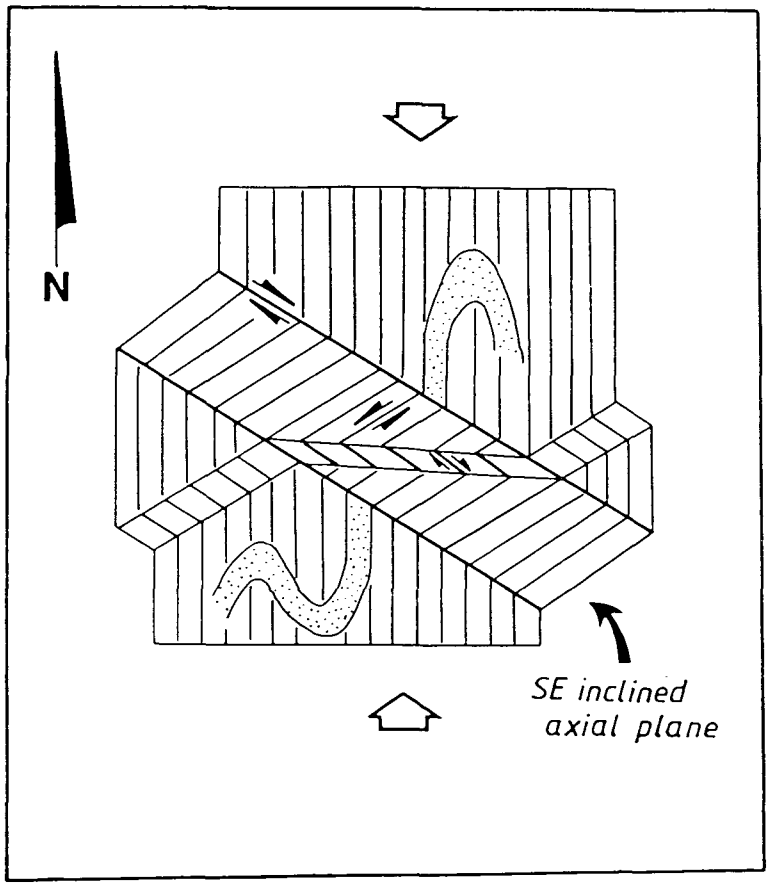

Fig. 2.17 Kink zone model for the formation of shear foliations in the Anamarra granite domain and lateral dextral shear zones in the Ongeva granulites, during the later stages of D_3. The predominace of southeast-trending dextral zones arises from differently directed and differently valued shear strains parallel to kink surfaces (from Ramsay and Huber, 1987).

northnortheast (~021), which is about 15° to the north of D_3 fold axes and L_4 in D_4 shear zones. L_5 has also been deformed by subsequent deformation. The change in orientation between D_3 fold axes and L_5 may indicate a slight rotation in principal stress directions during the deformation cycle (D_3-D_5). However, deformation in these zones could also be conceivably unrelated to D_3-D_4.

The similarity in orientation of structural fabric elements during D_3-D_5 suggests that they were produced during a continuous progressive deformational cycle. Progressive non-coaxial deformation during D_3 probably coincides with the "Proterozoic reworking" of Goscombe (1991). The later part of D_3 is characterized by axial symmetrical shortening. D_4-D_5 represent the partitioning of strain into narrower zones during cooling. D_3-D_5 deformation postdated the peak metamorphism and was unlike the inferred deformation mechanisms during D_1-D_2. This second major deformational cycle was probably associated with crustal shortening and is herein referred to as the *Arunta Orogeny*.

CHAPTER 3

Metamorphic evolution of the Strangways Metamorphic Complex: evidence from metapelites

Summary

Evidence for two metamorphic events (M_1, M_2) is shown by granulite facies rocks from the Ongeva granulites and the Anamarra granite domain, which belong to the Strangways Metamorphic Complex. Low-pressure granulite facies metamorphism, M_1, accompanied D_1/D_2, at conditions of P = 5.3±1.2 kbar and T>750°C. The effects of M_1 in metapelites are characterized by spinel+quartz-bearing assemblages, with enveloping S_{2b} sillimanite-biotite-magnetite assemblages implying near isobaric cooling. The effects of M_2 are characterized by S_1/S_2 cordierite pseudomorphed by orthopyroxene-sillimanite-biotite-magnetite symplectites, at conditions of P = 7.5±0.8 kbar and T~800°C. This retrograde *increase* in pressure was probably the result of crustal thickening during D_3, which produced northeast-plunging F_3 and F_4 folds in the Ongeva granulites and the Anamarra granite domain (Chapter 2). The increase in pressure with M_2 may reflect the beginning of a clockwise P-T-t path typical of collisional-style tectonics. Sillimanite-bearing, and orthopyroxene-bearing ultramylonites were produced during D_4, which was an extension event parallel to the D_3 transport axis and possibly related to crustal collapse after thickening during D_3[3].

[3] Norman, A. R. and Clarke, G. L., 1990. A barometric response to late compression in the Strangways Metamorphic Complex, Arunta Block, central Australia. *Journal of Structural Geology*, **12**, 667-684.

3.1 Introduction

High-grade Precambrian terrains dominate the continental fragments of Gondwana, and record the tectonic events that could be responsible for the formation of the supercontinent. However, the geological setting of these Precambrian tectonic events is commonly obscured by dislocation during much younger, unrelated tectonic events. In the absence of observed basement and/or tectonic margins, the deformation history of a terrain may be preserved in superimposed mineral fabrics, and the pressure-temperature (P-T) history preserved in successive mineral assemblages that constitute the mineral fabrics. The metamorphic/deformation history may be expressed as a P-T-time (t) path, with the absolute timing of events constrained by geochronology. In such terrains, the timing of the peak of metamorphism, with respect to deformation, provides a critical basis for assessing the tectonic setting of a deformation event. However, tectonic interpretations in many granulite facies Precambrian terrains are hampered because intense deformation and recrystallization has destroyed fabrics that predate the last metamorphism/deformation (e.g. Clarke and Powell, 1991).

The tectonic setting of regional metamorphism in the Phanerozoic usually invokes models of continental collision. Intense sub-horizontal and upright foliations, geometrically specific to the axis of convergence (Shackleton and Ries, 1984), reflect the deformation processes that result in crustal overthickening and metamorphism (e.g. Caby et al., 1983; LeFort, 1975; Windley, 1985). The mountain belt is assembled in less than the thermal time constant of the lithosphere (England and Richardson, 1977), and the agency by which metamorphism is terminated may be erosion (England and Richardson, 1977) or extension (England, 1987). The post-collisional thermal history for the assembled mountain belt may be complex (e.g. Sandiford, 1989b) but a common inference made from rock fabrics is that compressive deformation precedes both the thermal peak of metamorphism and near isothermal uplift (e.g. Selverstone et al., 1984) that returns the rocks to the earths' surface. Thus a *'clockwise' P-T-t path* is inferred.

Deriving a collisional tectonic setting to account for the metamorphic history in many granulite facies Precambrian terrains is difficult because of the thermally perturbed nature of the peak metamorphism, and the common inference that deformation, which is usually compressive (e.g. Clarke et al., 1986), occurred during cooling at constant, or slightly increasing pressure after peak metamorphism (e.g. Phillips and Wall, 1981; Warren, 1983a; Clarke et al., 1987, 1989b; Harley 1989). Either *isobaric cooling* or an *'anti-clockwise' P-T-t path* is inferred, and the terrain is interpreted as having remained at depth subsequent to metamorphism (Harley, 1989). In places, mapped isograds of Precambrian metamorphism/deformation (e.g. Hobbs et al., 1984) indicate that Precambrian deformation events resulted in a locally complex, but regionally minimal, disruption to stratigraphy or regional geology (e.g. Clarke et al., 1986, 1989). These effects are in contrast with large displacements (100 km) observed in Phanerozoic collisional orogens (e.g. LeFort, 1975). Although simple isobaric cooling may reflect several tectonic settings (Sandiford and Powell, 1986; Ellis 1987; Harley, 1989), isobaric cooling accompanying compressive deformation is more probably part of an anti-clockwise P-T-t path. An anti-clockwise P-T-t path can be explained by passive crustal thickening subsequent to crustal extension (Stüwe and Powell 1989a), or by thermally weakened crust responding to existing regional stresses. Such settings involve the access of abnormal amounts of heat from local felsic intrusions or mafic magmas in the lower crust, from lithospheric extension (Sandiford and Powell, 1986), or from fluid advection. In many areas, heat was probably transferred to the middle and upper crust from the mantle by advection (Wells, 1980; Thompson and Ridley, 1987; Vernon et al., 1990).

This Chapter presents an introduction to the metamorphic history of a portion of the Strangways Metamorphic Complex. By relating the observed mineral assemblages to the rock fabrics, the rocks are inferred to record both styles of P-T-t path outlined above and thus show successive metamorphisms indicative of different tectonic settings. Evidence is presented for an earlier, low-pressure metamorphism (M_1) that probably corresponds to a widely reported early Proterozoic granulite facies event (Warren, 1982; Black et al., 1983) and a subsequent retrograde moderate-pressure metamorphism (M_2).

A significant increase in pressure during M_2 is linked to a widespread folding episode (D_3, Chapter 2).

In this Chapter, evidence from successive mineral assemblages in metapelitic gneisses from the Ongeva granulites (Shaw et al., 1984a) and the Anamarra granite domain (Norman and Clarke, 1990) are used to interpret a portion of the metamorphic evolution of the Strangways Metamorphic Complex. The general geology of the area is shown in Fig. 1.1, and the relationship between deformation and metamorphic events is shown in Table 3.1.

As outlined in the introduction, the Anamarra granite domain is distinguished from the Ongeva granulites by containing deformed megacrystic granite, orthogneisses and metagabbro. Blocks of interlayered gneisses comprising folded quartzofeldspathic gneisses, mafic granofelses and minor cordierite gneisses, similar to gneisses in the Ongeva granulites also occur in the Anamarra granite domain. Metapelitic gneisses in the Ongeva granulites and Anamarra granite domain contain the same mesoscopic structures and mineral fabrics, and microscopic mineral assemblages indicative of a coeval structural and metamorphic evolution.

3.2 Geological setting

The Ongeva granulites and gneissic blocks in the Anamarra granite domain consist of interlayered quartz-feldspar±orthopyroxene±garnet-biotite gneisses, two pyroxene-hornblende-plagioclase granofelses, quartz-K-feldspar-sillimanite-garnet-biotite gneisses and minor calc-silicate rocks. The variation in bulk rock composition is defined by cm to m-scale layers. However, this compositional layering is commonly disrupted by orthogneiss in the Anamarra granite domain. These compositional layers may reflect a primary sedimentary layering, although they have been commonly boudinaged due to deformation and has been referred to as S_1 (Chapter 1, Chapter 2). Felsic granofelses and gneisses are interlayered with mafic gneisses and granofelses in the Ongeva granulites and in the eastern part of the Anamarra granite domain. They generally form

Table 3.1 Summary of the deformation and metamorphic history of the Strangways Metamorphic Complex, showing the correlation between deformation and metamorphic events (from Norman and Clarke, 1990).

DEFORMATION	FOLDING EVENTS	METAMORPHIC EVENT	PARAGENESES * mafic gneiss	felsic gneiss	metapelites	calc-silicate rocks	interpreted age constraints	suggested correlation of events with Warren (1983)
D_1	F_1 (S_1)	M_1	Opx-Cpx-Pl-Hbl ±Qtz±Bt	Opx-Pl-Qtz-Kfs ±Grt±Cpx	Sil-Spl-Qtz-Ilm-Pl -Kfs±Grt±Crd	Wol-Scp-Pl-Cpx -Qtz	1860 ±80 Ma[1] 1790 ±35 Ma[2]	**granulite stage** P = 8± 1 kbar, T = 850-920°C
D_2	F_2 isoclinal, intrafolial, rootless folds (S_2)		Opx-Pl (S_2) Hbl-Mag	Qtz-Kfs-Opx-Grt (S_2) Bt-Mag	Crd-Grt-Sil-Qtz -Kfs±Spl (S_2) Sil-Bt-Mag±Grt (S_{2b})	An-Qtz Grs-Qtz	1765 ± 4 Ma[3] 1745 ± 4 Ma[3]	**biotite stage**
D_3	F_3, F_4 isoclinal and open inclined, NE-plunging, SE-inclined folds	M_2	Cpx-Pl±Opx±Hbl	Hbl-Bt-Mag-Pl ±Scap	Opx-Sil-Bt-Mag ±Grt±Spr	Grt (And)	1470 ± 60 Ma[1]	
D_4	ultramylonitisation		Cpx-Opx-Pl-Hbl	Opx-Bt-Pl-Qtz	Sil-Bt-Pl-Qtz±Grt	Scp-Pl-Cpx-Grt -Qtz±Hbl		
D_5	deformation within the Gough Dam Schist Zone south-directed thrusting		Ged-Ath		Sil-Bt-Qtz-Kfs-Pl Ky-St-Bt		1750 Ma[4,5] 1450-1400 Ma[2,6]	**kyanite-gedrite stage** P ~ 8 kbar, T = 650-720°C
	late-Proterozoic uplift						1000 Ma[7]	**cordierite-kyanite-gedrite stage** Crd coronas on Ky and Sil isothemal uplift of 3-4 km
	green schist facies retrogression Arltunga Nappe Complex		Chl		Ms±Chl±Ep	Ep-Zo	mid-Carboniferous[8]	terrain remained at depth until the Alice Springs Orogeny

* mineral abbreviations after Kretz (1983)

[1] Iyer et al. (1976) [2] Black et al. (1983) [3] Norman and Collins (unpublished U/Pb zircon ages) [4] Mortimer et al. (1987)
[5] Cooper et al. (1988) [6] Allen and Stubbs (1982) [7] Windrum and McCulloch (1986) [8] Forman et al. (1967)

layers between 1 and 100 metres thick. Mafic gneisses and granofelses outcrop predominantly in the Ongeva granulites, forming about fifty percent of the outcrop. Mafic layers up to 10 cm thick occur in the felsic rocks and commonly form rootless, intrafolial, F_2 isoclinal folds; however, units up to 50 metres wide also occur. Calc-silicate rocks and marbles are not common, but occur interlayered with metapelitic gneisses. In some metapelites and mafic granofelses, calc-silicates form isolated boudins or impersistent layers of folded rock.

The Ongeva granulites and the Anamarra granite domain record three major folding episodes (F_2-F_4) subsequent to a high-temperature, low-pressure, granulite facies metamorphism (M_1) and followed by high-grade mylonitization (D_4, Table 3.1). Anatexis accompanied the granulite facies metamorphism. Evidence of an S_1 tectonometamorphic foliation has been largely obliterated because of recrystallization during D_2, which produced the pervasive S_2 foliation, shown as trend lines in Fig. 1.1. In metapelites, fine-grained sillimanite inclusions and inclusions of spinel-ilmenite in granoblastic cordierite and garnet are folded (F_2) and define an S_1 foliation. In cordierite-rich gneisses, a rare S_1 cordierite foliation is boudinaged and isoclinally folded by F_2, with quartz-K-feldspar-cordierite leucosomes forming axial-plane foliations. An S_2 foliation is generally defined by abundant, medium-grained quartz-K-feldspar±cordierite±garnet leucosome in metapelitic rocks. These leucosome layers are inferred to have crystallized from partial melt during cooling after the metamorphic peak. S_2 is axial-planar to rootless, intrafolial, isoclinal F_2 folds (Chapter 2) and is mostly subparallel to the compositional layering (S_1). The crystallization of partial melts in the axial-planes of F_2 folds and boudinaged mafic layers in felsic gneisses probably represent the effects of a ductile non-coaxial deformation during D_2 after the peak of metamorphism (Chapter 2).

In metapelitic gneisses, a coarse-grained sillimanite-biotite-magnetite foliation cuts the main S_2 quartz-K-feldspar±cordierite±garnet leucosome layering (Fig. 3.1a), but is generally sub-parallel to the overall trend of S_2. This sillimanite-biotite foliation is

Fig. 3.1 (a) Coarse-grained S_{2b} sillimanite-biotite foliation, Ongeva granulites.

3.2 (b) Irregularly-shaped, coarse-grained, pegmatitic pod of garnet-K-feldspar-quartz-biotite cutting S_{2b} sillimanite foliation and calc-silicate boudins, Ongeva granulites.

3.1 (c) S_{2b} sillimanite foliation and S_2 cordierite-quartz leucosome (arrowed) tightly folded by F_3 with some sillimanite reoriented into the axial plane, Anamarra granite domain.

3.1 (d) Irregular pegmatitic network of plagioclase-hornblende-orthopyroxene cutting S_2 in a mafic granofels, Ongeva granulites.

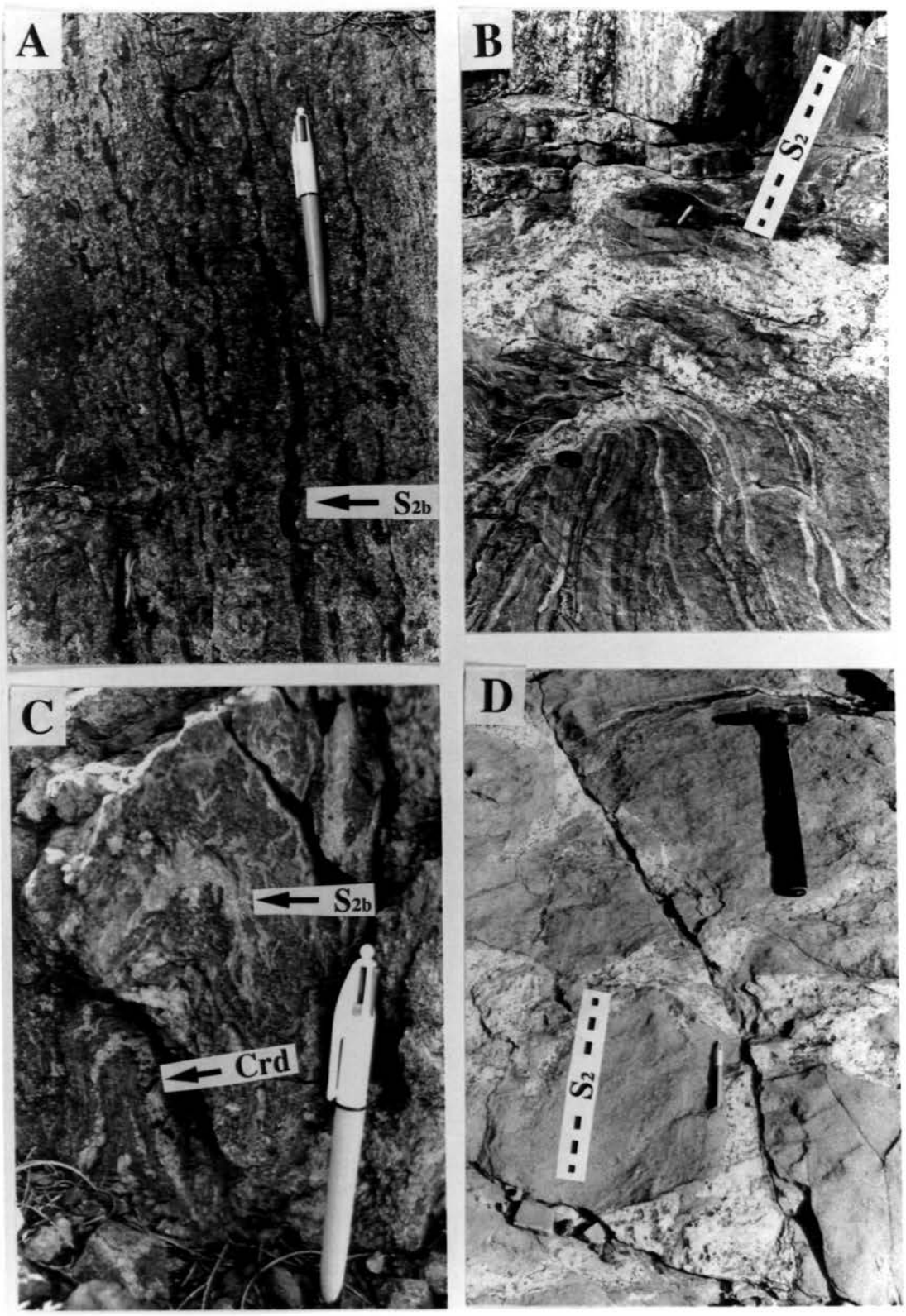
A
S2b
B
S2
C
S2b
Crd
D
S2

designated as S_{2b}. Sillimanite in this foliation is poorly lineated. Large, irregularly-shaped, coarse-grained pegmatitic pods of garnet-K-feldspar-quartz-biotite (Fig. 3.1b) cut the sillimanite-biotite S_{2b} foliation but also commonly contain a poorly-developed biotite foliation that is parallel to S_2/S_{2b}. These relationships are inferred to represent the continual crystallization of melt and mineral reactions as a response to cooling from peak metamorphism (M_1) as the effects of D_2 waned.

Although macroscopic fold patterns are rarely evident in the Anamarra granite domain due to extensive dissection by shear foliations, three mesoscopic folding phases can be recognized in metapelitic gneisses, which are similar to F_2-F_4 in the Ongeva granulites. S_2 and S_{2b} and pegmatitic pods are folded by northeast-plunging, discontinuous, tight to isoclinal F_3 folds and open, plunging, inclined asymmetric F_4 folds. F_3 and F_4 folds are colinear, and both have a northwest sense of vergence, suggesting that they were the product of a single deformation event, which has been designated as D_3. Minor quartz-K-feldspar-garnet leucosomes occur parallel to the axial-planes to F_3 folds. In places, coarse-grained pegmatite occurs between boudins on the limbs of F_3 folds. Minor quartz-K-feldspar leucosome crystallized in conjugate shear sets on the limbs of F_4 folds, indicating the continual crystallization of leucosome from melt throughout D_3.

F_4 folds are cut by coarse-grained quartz-K-feldspar-biotite pegmatite dykes. Some pegmatite dykes contain biotite which is elongate, parallel to the F_4 axial-planes, suggesting that intrusion was syndeformational. A late-D_3 pegmatite is shown in Fig. 3.2, which contains xenoliths derived from adjacent metapelites and biotite parallel to F_4 axial-planes. Xenoliths in this pegmatite dyke are important because they contain assemblages associated with an M_2 metamorphism (see petrography) and therefore place constraints of the timing of M_2 relative to pegmatite emplacement and F_4 folding.

F_4 folds and pegmatite dykes are cut by shear zones that represent the effects of D_4. These shear zones are characterized by narrow, east-trending discrete zones of high-grade ultramylonite, which have a consistent north-side down sense of shear and

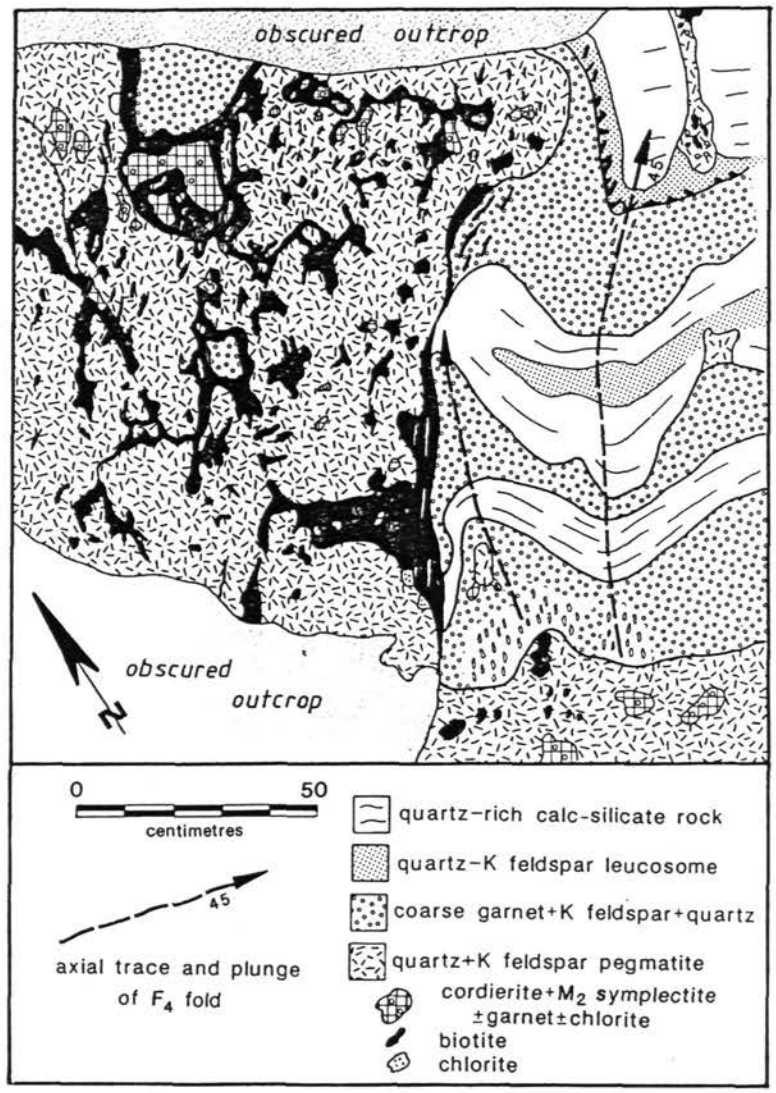

Fig. 3-2 Outcrop sketch of open F_4 folds and late D_3 quartz-feldspar-biotite pegmatite containing xenoliths of cordierite with M_2 symplectic aggregates (from Norman and Clarke, 1990).

generally displace F_3 and F_4 folds (Norman, 1989; Norman and Vernon, 1991; Chapter 5).

3.3 Geochronological constraints

On the basis of petrography and Rb-Sr isotopic data, Iyer et al. (1976) suggested that the Strangways Metamorphic Complex was affected by two distinct granulite facies metamorphic events: one at 1860±80 Ma and another at 1470±60 Ma. These events probably correspond to M_1 and M_2 recognized in this thesis since the corona and pseudomorphous textures described by Iyer et al. (1976) are similar to the M_2 textures, which are described in this Chapter. Black et al. (1983) inferred several events also from Rb-Sr isotopic data, with a corresponding early granulite facies event at 1790±35 Ma. Allen and Stubbs (1982) also interpreted multiple recrystallization events from Ar^{40}/Ar^{39} data, with a similar early granulite facies event and a thermal pulse at about 1450 Ma.

Gross disturbances to the Rb/Sr and Ar^{40}/Ar^{39} isotopic systems of rocks in the Strangways Metamorphic Complex also appear to have occurred in the period 1400-1000 Ma (Iyer et al., 1976; Allen and Stubbs, 1982; Black et al., 1983). Multiple deformations and metamorphisms have almost certainly disturbed the isotopic system of the rocks several times but it is almost impossible to be certain to what event(s) the reported younger isotopic ages correspond. The problem is further compounded by the extensive, probably multiply worked, retrograde shear zones (D_5) that bound the Strangways Metamorphic Complex. In addition, much of the Rb/Sr and Ar^{40}/Ar^{39} work is contradicted by U/Pb studies (Mortimer et al., 1987; Cooper et al., 1988), which suggest that shearing occurred around 1750 Ma and that no isotopic disturbances of the system occurred until ~500 Ma. This implies that M_2 occurred before 1750 Ma. All that we can be certain about is that the rocks were exposed when the late-Proterozoic Heavitree Quartzite was deposited in the Amadeus Basin.

The Alice Springs Orogeny in the mid-Carboniferous resulted in the further dislocation of the high-grade terrain, probably along reactivated shear zones (Stewart,

1971; Collins and Teyssier, 1989). Coarse-grained muscovite and chlorite±epidote foliations cut shear foliations in the Anamarra granite domain and biotite foliations in the Gough Dam Shear Zone and may be associated with the later Palaeozoic event(s). The geochronological data are also summarized in Table 3.1.

3.4 Metamorphic geology

This section is primarily concerned with metapelitic rocks, because they are the most useful for inferring the barometric metamorphic history in the Strangways Metamorphic Complex. However, metapelites are relatively uncommon in both the Ongeva granulites and the Anamarra granite domain; so the interlayered felsic and mafic gneisses calc-silicate rocks are also briefly described in this Chapter. Chapter 4 contains more detailed descriptions of mineral compositions in felsic, mafic and calc-silicate rocks, which help refine the P-T-t path interpreted from metapelites in this Chapter. Much of the tectonometamorphic history is also contained in the shear zones that transect and bound the Strangways Metamorphic Complex. Descriptions of mineral fabrics in shear zones transecting the Strangways Metamorphic Complex are discussed in more detail in Chapter 5 and mineral fabrics in the bounding shear zones are discussed in Chapter 6 and by Warren (1983a).

The rocks are interpreted to have been affected by two granulite facies metamorphic events, M_1 and M_2, and the relationship between the deformation events and these metamorphisms is summarized in Table 3.1. The mineral assemblages in felsic gneisses, mafic granofelses and calc-silicate rocks indicate that metamorphic conditions reached granulite facies grade (Turner, 1968) during the early part of the tectonic history of the Strangways Metamorphic Complex (D_1) and probably remained at granulite facies conditions during D_2. The effects of M_2 are easily recognized in metapelites and clearly post-date the cordierite-bearing S_2 leucosome and S_{2b} sillimanite-biotite foliation. Cordierite-bearing xenoliths in a syn-F_4 pegmatite (Fig. 3.2) contain M_2 assemblages which suggests that M_2 occurred before F_4. D_4 ultramylonitization probably occurred at

granulite facies conditions (Norman, 1989; Norman and Vernon, 1991; Chapter 5) and also post dated M_2.

3.41 Petrography

Metapelites

Metapelites, which have a rust-red outcrop colour, are characterized by abundant sillimanite, garnet and biotite, and commonly grade into quartz-feldspar-biotite migmatites. The most obvious foliation in these rocks consists of poorly-lineated, coarse-grained sillimanite, large biotite grains and magnetite (S_{2b}). Medium to coarse-grained K-feldspar-quartz±cordierite±garnet±biotite leucosome layers, which delineate the main S_2 foliation, are cut by this coarse-grained sillimanite S_{2b} foliation (Fig. 3.1a). Corundum is a minor mineral occurring with sillimanite, but isolated from quartz and feldspar by either biotite or sillimanite. This foliation is interpreted as forming late in D_2, due to a flattening strain. The coarse-grained sillimanite-biotite-magnetite S_{2b} foliation is tightly folded by F_3 folds (Fig.3.1c; Fig. 3.3a) and is cut by D_4 ultramylonite zones (Fig. 3.3b). Garnet may occur as large, irregular, elongate, poikioblastic or idioblastic grains in S_2 leucosome layers, but may also envelop the coarse-grained sillimanite foliation. Coarse-grained garnet also occurs in quartz-K-feldspar-biotite pegmatite pods that cut S_2 and S_{2b}. Garnet appears to have been present at M_1 and throughout D_2. Garnet that is elongate in the S_2 foliation may contain folded inclusions of fine-grained sillimanite suggesting that sillimanite was part of the S_1 assemblage and that S_2 is a tectonic fabric.

Coarse-grained magnetite occurring with S_{2b} sillimanite invariably contains subidioblastic inclusions of spinel (Fig. 3.3c), which may contain idioblastic inclusions of ilmenite (Fig. 3.4). Spinel also occurs as inclusions in coarse-grained sillimanite and garnet. Coronas of sillimanite around spinel are also observed in garnet quartz-feldspar gneisses. Spinel and ilmenite are inferred to have formed part of the peak assemblage in metapelites, with sillimanite, magnetite and biotite produced during retrogression.

Fig. 3-3 (a) S_{2b} sillimanite and magnetite isoclinally folded by F_3 in a cordierite gneiss from the Anamarra granite domain. Sample 372. Base of photograph is 4.4 mm.

3.3 (b) Coarse-grained S_{2b} sillimanite foliation truncated by a D_4 ultramylonite zone, Ongeva Granulites. Sample 377. Base of photograph is 12.0 mm.

3.3 (c) S_{2b} magnetite containing M_1 spinel inclusions. Note the coarse-grained S_{2b} sillimanite and the enveloping M_2 orthopyroxene-sillimanite-biotite symplectite, Ongeva Granulites. Sample 106. Base of photograph is 1.75 mm.

3.3 (d) M_2 orthopyroxene-sillimanite -biotite-magnetite symplectite replacing cordierite along its grain boundaries. Symplectite encloses S_{2b} magnetite which has a M_1 spinel inclusion, Anamarra granite domain. Sample 257. Base of photograph is 4.4 mm.

3.3 (e) Vermicular intergrowth of magnetite with M_2 orthopyroxene-sillimanite-biotite symplectite, Anamarra granite domain. Sample 702. Base of photograph is 0.7 mm.

3.3 (f) M_2 orthopyroxene-plagioclase corona at the interface of hornblende and plagioclase and ferroan pargasite at the interface of orthopyroxene and plagioclase in a mafic granofels from the Ongeva granulites. Sample 375. Base of photograph is 1.75 mm.

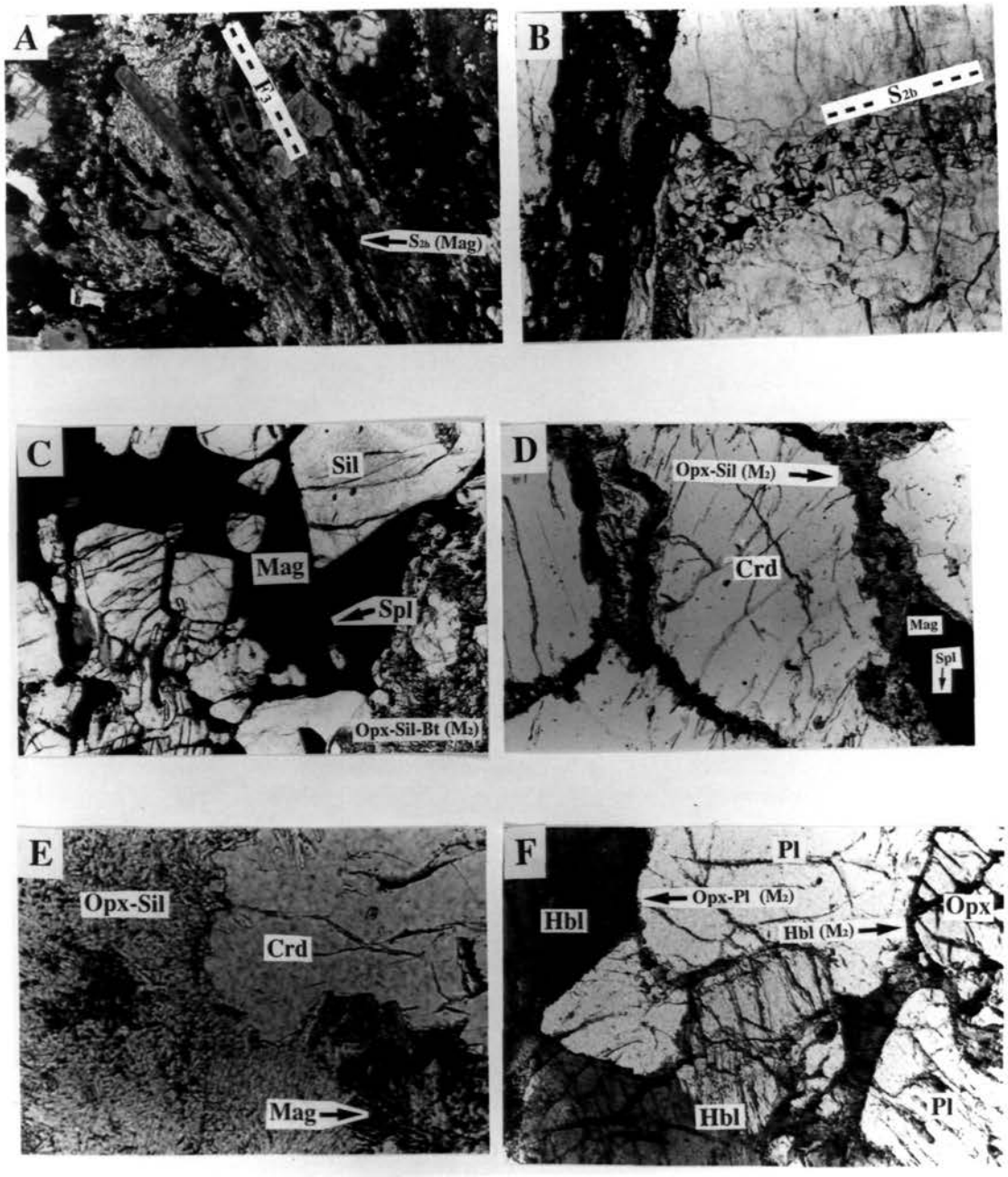
A
S_{2b}
S_{2b} (Mag)
B
S_{2b}
C
Sil
Mag
Spl
Opx-Sil-Bt (M_2)
D
Opx-Sil (M_2)
Crd
Mag
Spl
E
Opx-Sil
Crd
Mag
F
Pl
Opx-Pl (M_2)
Opx
Hbl
Hbl (M_2)
Hbl
Pl

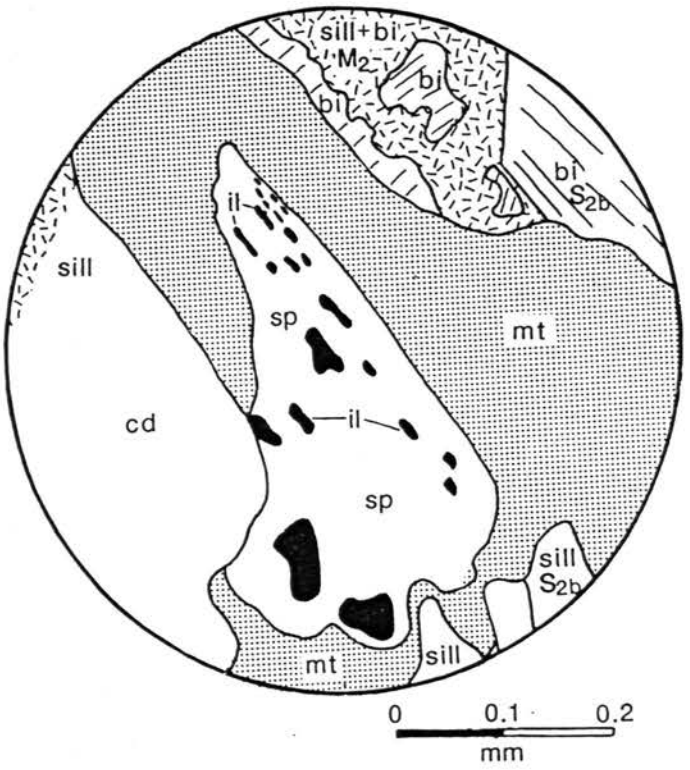

Fig. 3-4 Diagram from a back-scatter electron image of an S_{2b} magnetite containing a M_1 spinel inclusion, which has inclusions of ilmenite, Anamarra granite domain (from Norman and Clarke, 1990). Sample 709.

In cordierite-rich gneisses, spinel also occurs as inclusions in medium-grained granoblastic cordierite, which occurs with quartz in S_2, and is enveloped and cut by coarse-grained S_{2b} sillimanite, biotite and magnetite. Small fine-grained sillimanite needles are contained in some garnet and cordierite grains, forming inclusion trails that are folded (F_2) or at a high angle to the enveloping and cross-cutting S_{2b} sillimanite foliation. Hence, cordierite is interpreted as having been present with spinel, ilmenite, K-feldspar, garnet, sillimanite and quartz at peak metamorphic conditions of M_1. As in the felsic gneisses, quartz commonly has undulose extinction and is extensively recrystallized, feldspar has recrystallized grain boundaries, and large S_{2b} biotite grains are commonly kinked.

In some metapelites, cordierite has been replaced along its grain boundaries and cleavage planes by poorly-oriented, fine-grained symplectic aggregates of orthopyroxene-sillimanite-biotite-magnetite (Fig. 3.3d). In most metapelites from the Ongeva granulites, the orthopyroxene-sillimanite-biotite-magnetite symplectite (±sapphirine) commonly totally pseudomorphs cordierite. The sillimanite is random, the orthopyroxene (av. $\%X_{Mg} = 58.1$, av. $Al_2O_3 = 6.49$ wt%, Table 3.4) is unaltered, and magnetite forms a vermicular intergrowth (Fig. 3.3e). Aluminous orthopyroxene may be expected to occur at high temperatures, in the presence of garnet (Harley, 1984b); however, it is more probable that, in places, the high Al content of orthopyroxene reflects excess alumina from the breakdown of cordierite not involving the matrix garnet, quartz and feldspar. Sapphirine occurring with some pseudomorphous symplectites supports this interpretation. Vermicular magnetite also occurs around the margins of garnet grains. Coarse-grained S_{2b} sillimanite has "beards" of fine-grained sillimanite and may be enclosed by the symplectite. The symplectic aggregates are fine-grained and quite distinct from the coarse-grained S_2 minerals, but are cut by the D_4 ultramylonite zones. Coexisting orthopyroxene and sillimanite imply higher pressure conditions than any of the mineral assemblages observed for S_1/S_2 (see petrogenetic grid). From this and their clear textural distinction, the metamorphic event responsible for the orthopyroxene-sillimanite-biotite-magnetite±sapphirine symplectite is designated as M_2.

This M_2 symplectite after cordierite has been found in cm-size xenoliths of cordierite gneiss in a syn-F_4 quartz-K-feldspar-biotite pegmatite dyke (Fig. 3.2). Biotite in this pegmatite is aligned parallel to the axial-planes of open F_4 folds. The surrounding folded rocks contain cordierite gneisses with similar M_2 assemblages. The field and microscopic observations indicate that M_2 occurred before F_4 folding and D_4 ultramylonitization but after the development of S_{2b}. Therefore, the pressure increase indicated by M_2 orthopyroxene-sillimanite assemblages after cordierite was probably a response to deformation associated with F_3 folding. That the rocks were not entirely recrystallized during this event presumably reflects a moderately low water activity.

Quartz-free assemblages

Silica-undersaturated rocks such as those described by Warren and Hensen (1987) from the northern tectonic zones have not been observed in this study area. However, quartz-free assemblages containing sapphirine, corundum and spinel exist on a microscopic scale. As mentioned above, primary spinel is preserved in retrograde magnetite and sillimanite, and in D_1/D_2 garnet and cordierite. Corundum occurs within biotite and sillimanite S_{2b} folia; quartz and feldspar are absent from these areas in the rock. Sapphirine occurs as small idioblastic to subidioblastic grains with sillimanite, orthopyroxene and biotite in the M_2 symplectites contained in the metapelitic gneisses. The presence of retrograde sapphirine is discussed in Chapter 4. Primary sapphirine as inclusions within cordierite has not been observed.

Felsic gneisses

The felsic gneisses vary from equigranular, medium-grained, granoblastic, quartz-rich, K-feldspar-plagioclase-orthopyroxene gneisses and granofelses to garnet-bearing, K-feldspar-quartz-orthopyroxene-biotite±clinopyroxene migmatites. The proportion of plagioclase varies considerably. The S_2 foliation is mainly defined by deformed, coarse-grained leucosome layers and the alignment of some biotite grains, although biotite may have largely crystallized during the development of the later S_{2b} foliation. The S_2

foliation contains boudinaged, large, subrounded K-feldspar grains, most probably remnants from D_1 (Fig. 2.1g). These large K-feldspar grains are contained in medium-grained, granoblastic leucocratic layers, which presumably crystallized from melt during D_2. Deformation features in S_2 leucocratic layers include: extensively recrystallized quartz grains, which show well-defined dentate grain boundaries; small subgrains and minor myrmekite around the margins of plagioclase; plagioclase grains with deformation twins and minor recrystallization. Similar deformation features are described from the Mount Schaber granofels in Chapter 1. These features post-date M_1 and S_2 assemblages and may be related to deformation late in D_2 or later recrystallization associated with D_3. Orthopyroxene is invariably rimmed by grey-blue hastingsitic hornblende. Hornblende and fine-grained biotite after orthopyroxene, together with a quartz mylonitic fabric form axial-plane foliations (S_3) to tight, intrafolial F_3 folds indicating that hydrous, mylonitic conditions existed early in D_3 (Fig. 2.6d) Garnet is generally poikiloblastic, with rounded inclusions of quartz and K-feldspar, and has small biotite grains along micro-cracks and around its margins. Large poikiloblastic garnet may also contain folded inclusion trails of spinel-ilmenite that define S_1 and F_2 folds (Fig. 2.1b). Large, brown biotite grains which are generally sub-parallel to S_2 leucocratic layers, are commonly kinked owing to post-D_2 deformation.

Mafic granofelses

A high-grade gneissic layering (S_2) is defined by alternating, medium-grained, hornblende-orthopyroxene-rich and plagioclase-rich layers. Thin plagioclase-rich layers may contain subidioblastic, coarse-grained orthopyroxene or coarse-grained hornblende aligned in this S_2 foliation. The mesosomes have a granoblastic texture consisting of orthopyroxene, clinopyroxene, green-brown hornblende, plagioclase and magnetite. Hornblende may form up to 70% of the mafic layers. The S_2 layering is sub-parallel to the gross compositional layering (S_1) and axial-planar to F_2 folds. A thin, granoblastic, two-pyroxene S_1 layering is folded by F_2. Granulite facies conditions, as evidenced by the two-pyroxene assemblages, existed at peak metamorphism (M_1-D_1) and persisted

during D_2. The main, penetrative S_2 foliation is cut by irregular networks of coarse-grained orthopyroxene-plagioclase-rock that may contain a weak foliation parallel to S_2. These coarse- grained networks may be coeval with similar garnet-bearing pegmatite pods in metapelites and orthopyroxene-bearing pods in felsic granofels that cut S_2 (Fig. 3.1d) but are folded by F_3. These pegmatite pods and networks appear to have crystallized from melt early in D_3 or late in D_2. Orthopyroxene in these late-D_2 pegmatites is invariably rimmed by grey-blue pargasite.

Coarse-grained granoblastic minerals in mafic gneisses and granofelses commonly exhibit recrystallized grain boundaries and interface symplectites. Coarse-grained hornblende grains have coronas of granular, subidioblastic orthopyroxene and plagioclase where in contact with plagioclase grains (Fig. 3.3f). Clinopyroxene is usually recrystallized around its margins and orthopyroxene is rimmed by ferroan pargasite (Fig. 3.3f). These corona and recrystallization textures are cut by D_4 ultramylonites and are inferred to be the effects of M_2. The effects of M_2 in mafic rocks is discussed more fully in Chapter 4.

Calc-silicate rocks

Calc-silicate rocks preserve a high-grade S_2 gneissosity defined by alternations in the proportion of quartz-rich layers and scapolite-wollastonite-clinopyroxene-anorthite-garnet layers. This layering is parallel to the regional compositional layering (S_1). S_2 is medium-grained and granoblastic. Other minor minerals in S_2 include calcite, quartz, sphene and magnetite. Scapolite invariably has recrystallized grain margins, and both clinopyroxene and plagioclase have coronas of garnet. In wollastonite-rich rocks scapolite also has a corona of garnet and the wollastonite occurs as large xenoblastic grains. Clinopyroxene shows undulose extinction, and quartz-rich layers show extensive recrystallization. The garnet coronas are post metamorphic peak and may be related to cooling during D_2 or to M_2. Rare calcite-rich rocks may occur interlayered with the calc-silicates. These marbles are medium-grained and contain diopside, scapolite, garnet , spinel and phlogopite.

D_4 ultramylonites

D_4 shear zones containing ultramylonite transect the D_3 structures. The ultramylonite is of variable composition and may show neocrystallization of sillimanite and biotite and recrystallization of orthopyroxene, clinopyroxene, garnet and hornblende (Chapter 5). Marble breccia, which occurs between some ultramylonite zones contains folded fragments of ultramylonite, recrystallized calcite and inclusions of scapolite and K-feldspar with garnet coronas (Norman, 1989). This marble is inferred to have been ductile during D_4 ultramylonitization. Inclusions of scapolite and K-feldspar with garnet coronas in the marble implies that the corona textures developed prior to D_4 ultramylonitization.

Summary

In the Ongeva granulites and the Anamarra granite domain, M_1 is characterized by a two pyroxene-hornblende-plagioclase assemblage in mafic rocks, quartz-K-feldspar-orthopyroxene±garnet in felsic rocks and wollastonite-scapolite-clinopyroxene-anorthite in calc-silicate rocks. Although a primary assemblage in metapelites is difficult to recognize because of overprinting reactions that occurred during D_2-D_4, a probable primary M_1 assemblage is cordierite-sillimanite-garnet-spinel-ilmenite-quartz-K-feldspar. Anatexis was probably associated with peak metamorphism. Cooling from peak metamorphism was associated with the crystallization of partial melt into S_2 leucosome layers during D_2 in a ductile, non-coaxial regime and crystallization of irregular pegmatitic pods late in D_2 and early in D_3. The formation sillimanite-biotite S_{2b} assemblages in metapelites, towards the end of D_2, involved the hydration and retrogression of peak M_1 assemblages, probably represented by the reaction, cordierite + K feldspar = sillimanite + biotite + quartz. Possible sources of hydrous fluids may be from crystallizing partial melt or from the intrusion of granite in the Anamarra granite domain.

The effects of a second metamorphic event, M_2, are recognized by pseudomorph, corona and recrystallized textures to minerals occurring in S_2. Symplectic intergrowths

of orthopyroxene-sillimanite-biotite-magnetite±sapphirine pseudomorph cordierite in metapelitic gneisses, fine-grained clinopyroxene-plagioclase coronas occur on hornblende in mafic gneisses, and pargasitic to hastingsitic hornblende rims occur on orthopyroxene in mafic and felsic granofelses and gneisses. In calc-silicate rocks, garnet coronas around clinopyroxene, plagioclase and scapolite may also be the represent the effects of M_2 (Chapter 4). M_2 textures are cut by the D_4 ultramylonite zones. M_2 was probably associated with, and may have been in response to D_3 folding in the Ongeva granulites and the Anamarra granite domain.

Neocrystallization of sillimanite in ultramylonites indicates that conditions were hot (Norman, 1989) during D_4, and the persistence of orthopyroxene in the ultramylonites suggests that water activity was fairly low (c.f. Sandiford, 1985a). Granulite facies conditions probably existed during D_4 (Chapter 5).

3.42 A petrogenetic grid to account for the mineral assemblages

Characteristic mineral parageneses have been identified for different stages in the metamorphic and deformation history of the Strangways Metamorphic Complex. The relative P-T conditions of these mineral assemblages can be established using petrogenetic grids involving all the observed minerals (e.g. Hensen, 1971) and can be used to infer a P-T path followed by the rocks during their evolution. The inclusion of spinel, ilmenite and magnetite in the inferred mineral assemblages requires a consideration of the model system, K_2O-FeO-MgO-Al_2O_3-SiO_2-H_2O (KFMASH) augmented by the addition of Fe_2O_3 and TiO_2 (KFMASHTO). The extension of a KFMASH petrogenetic grid, which is applicable to granulite facies conditions, into KFMASHTO was presented by Clarke et al. (1989). This KFMASHTO grid has been used successfully to explain metamorphic assemblages and corona reaction textures in spinel-quartz-bearing rocks metamorphosed under similar conditions to the rocks comprising the Strangways Metamorphic Complex (Clarke et al., 1989, 1990; Stüwe and Powell, 1989a, 1989b). Sillimanite was present as part of the primary (M_1) assemblage and was involved in all the successive mineral assemblages in the metapelites described above, so the petrogenetic grid can be

simplified by projecting from sillimanite (Fig. 3.5). The location of the inferred metamorphic peak, S_2 and M_2 assemblages are indicated in Fig. 3.5 by shading.

The metapelites contain coarse-grained garnet, quartz, K-feldspar and cordierite, suggesting that they were part of the primary M_1 mineral assemblage. Remnants of spinel and ilmenite occur as inclusions in magnetite and garnet, suggesting that spinel and ilmenite were also present at peak conditions. Ilmenite is rare, and occurs only as inclusions; it is never in textural equilibrium with quartz and feldspar. Spinel is comparatively abundant, occurring as inclusions in magnetite, garnet, sillimanite and cordierite. The pervasive, coarse-grained S_{2b} sillimanite-biotite-magnetite foliation cuts through all these minerals. These textures are best explained by the rocks cooling through and reacting across reactions A and B in Fig. 3.5. They imply an approximately isobaric cooling path during D_2, but any change in pressure is poorly constrained. The early P-T-t path for rocks from the Strangways Metamorphic Complex is refined in Chapter 4, using mineral zoning. However, isobaric cooling or a limited change in pressure with cooling is implied by the absence of cordierite overgrowths on garnet, or garnet overgrowths on cordierite, which appear to form readily with decompression and compression (Stüwe and Powell, 1989a, 1989b), respectively.

In many metapelites, the late fine-grained orthopyroxene- sillimanite-biotite-magnetite symplectic aggregates totally pseudomorph a coarse-grained mineral. In places, remnant cores of cordierite are preserved. In some metapelites, this symplectic aggregate rims cordierite. The textures and inferred primary assemblages in metapelites are consistent between the Ongeva granulites and the Anamarra granite domain.

The pseudomorphous, fine-grained, orthopyroxene-sillimanite-biotite-magnetite symplectic aggregates are quite distinct from the coarse-grained S_{2b} sillimanite-biotite-magnetite foliation. The petrogenetic grid (Fig. 3.5) implies that conditions were at some considerably higher pressure during development of the M_2 symplectite than during crystallization of either the peak M_1 assemblage or the S_{2b} mineral assemblages; that is M_2 was at a greater pressure than reaction C and probably at a greater temperature than

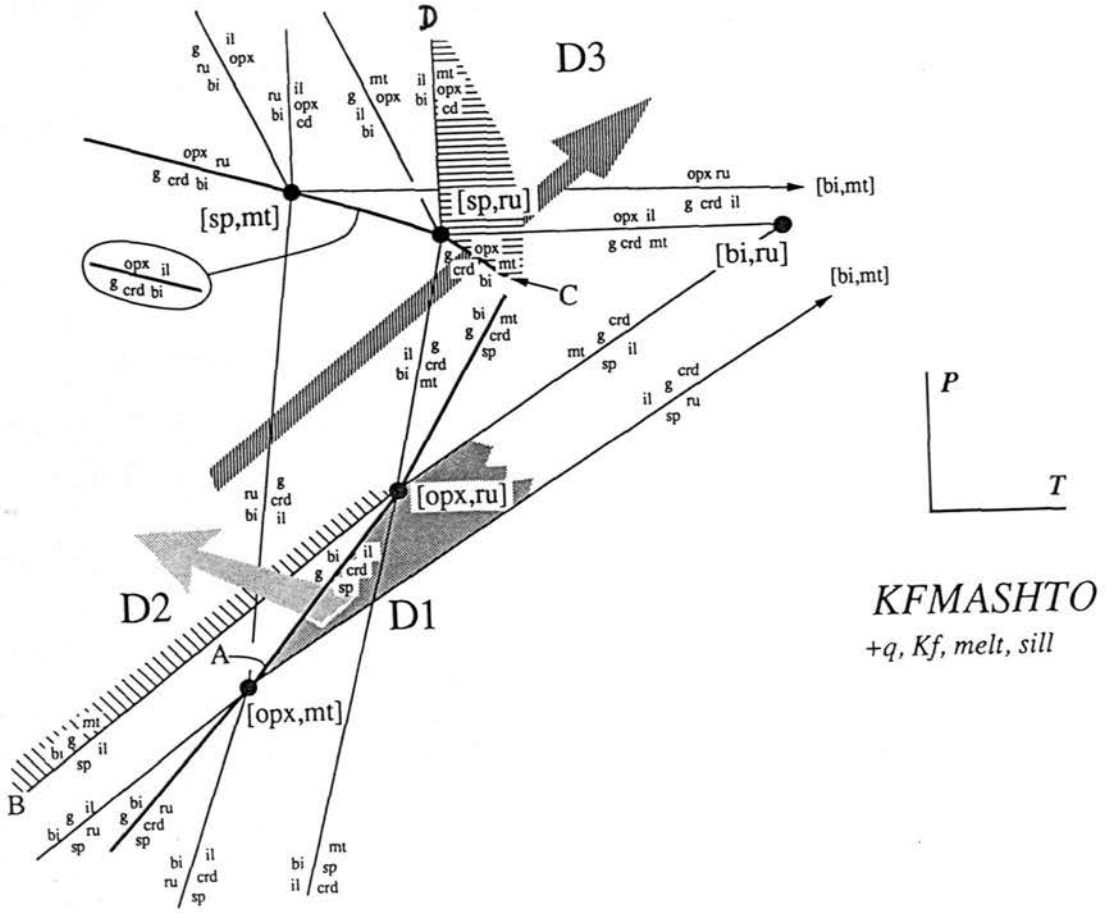

Fig. 3.5 K_2O-FeO-MgO-Al_2O_3-SiO_2-MgO-H_2O-TiO_2-O_2 (KFMASHTO) petrogenetic grid, for a projection from quartz, K-feldspar, sillimanite and melt, after Clarke et al. (1989). The shaded areas represent the metamorphic conditions implied by the peak (S_1), S_2 and M_2 (D_3) assemblages described in the text. The reactions marked as A, B, C and D are the reactions that are inferred to be involved in the development of the overprinting mineral assemblages. The large arrows show the inferred P-T path for the Strangways Metamorphic Complex: after approximately isobaric cooling from peak M_1 conditions, the terrain experienced an increase in pressure during the M_2-D_3 event. See Table 3.1 for the correlation between metamorphic and deformation events.

reaction D (Fig. 3.5). Cordierite was partly or wholly consumed in the development of the M_2 assemblage. It seems inescapable that the terrain suffered a late increase in pressure after the development of the S_{2b} foliation. Field evidence (Fig. 3.4) constrains this increase in pressure to occur sometime during D_3. The grid also suggests that the rocks experienced comparable, or slightly higher temperature conditions during this event than at the end of D_2 when the coarse-grained sillimanite foliation formed (Fig. 3.5).

Corundum occurs in the coarse-grained S_{2b} sillimanite foliation and, less commonly, idioblastic sapphirine occurs with the M_2 sillimanite-orthopyroxene symplectite. Corundum and sapphirine are never in contact with quartz and feldspar in the S_2 foliation; they are presumably the product of some local equilibrium, on a scale less than the width of the S_{2b} foliation or the diameter of the grains that the symplectites pseudomorphed.

3.43 Quantitative pressure estimates for M_1 and M_2

The mineral assemblages in metapelites described in the previous sections have potential for the estimation of conditions using the "average pressure approach" of Powell and Holland (1988), with the expanded internally consistent thermodynamic dataset of Holland and Powell (1990). Mineral analyses were obtained at Macquarie University using an ETEC electron microprobe with an accelerating voltage of 15 kV . Representative analyses of metapelitic assemblages are presented in Tables 3.2, 3.3, 3.4. The application of the average-pressure approach to these and similar metapelites (e.g. Clarke et al. , 1989), is complicated by the problem of re-equilibration during cooling, affecting mineral compositions (e.g. Fe-Mg exchange), even if the primary assemblage can be satisfactorily identified. Of course, the problem is compounded by the partial recrystallization of the metapelites during D_2 and D_3. These problems are particularly acute with respect to spinel, because extensive exsolution of magnetite has occurred during the development of S_2. Moreover, if biotite is to be effectively included in the calculations, the activity of H_2O is an extra variable. In the rocks considered here, which were partially melted at the metamorphic peak, a_{H_2O} was less or much less than unity.

Table 3.2 Representative microprobe analyses of minerals in sample 704.

wt%	Spl	Ilm	Crd	Kfs	Grt (core)	Grt (rim)	Sil (S_{2b})	Bt (S_{2b})	Opx (M_2)	Sil (M_2)
SiO_2	-	0.09	49.7	64.92	39.05	38.91	37.3	37.2	49.05	39.43
TiO_2	-	51.49	-	-	-	-	-	3.09	-	-
Al_2O_3	59.79	0.19	33.36	18.71	22.02	22.42	62.39	15.57	6.42	52.93
Cr_2O_3	0.34	-	-	-	-	-	-	0.08	-	-
FeO	27.53	42.12	3.7	-	30.23	30.69	0.97	15.14	23.93	4.01
MnO	0.09	3.74	-	-	0.42	0.61	-	-	0.44	-
MgO	8.12	0.36	11.23	-	8.52	8.96	-	14.82	19.87	2.88
CaO	-	-	-	0.1	1.29	0.26	-	0.05	0.11	-
Na_2O	0.04	-	0.19	2.08	-	0.26	-	0.46	-	-
K_2O	-	-	-	13.59	-	-	0.04	9.53	-	-
ZnO	5.17	-	-	-	-	-	-	0.08	-	-
TOTAL	101.08	97.99	98.18	99.4	101.53	101.85	100.7	96.02	99.82	99.25
Structural analysis										
basis of	4 (O)	3 (O)	18 (O)	32 (O)	24 (O)	24 (O)	5 (O)	22 (O)	6 (O)	5 (O)
Si	-	0.00	5.02	11.96	5.98	5.94	1.01	5.53	1.84	1.10
Ti	-	0.99	-	-	-	-	-	0.35	-	
Al	1.94	0.01	3.96	4.06	3.97	4.03	0.02	2.72	0.28	1.730
Cr	0.01	-	-	-	-	-	-	0.01	-	-
Fe	0.63	0.90	0.31	-	3.87	3.92		1.88	0.75	0.09
Mn	0.00	0.08	-	-	0.06	0.08	-	-	0.01	-
Mg	0.33	0.01	1.69	-	1.95	2.04	-	3.28	1.11	0.12
Ca	-	-	-	0.02	0.21	0.04	-	0.01	0.01	-
Na	0.00	-	0.04	0.74	-	-	-	0.13	-	-
K	-	-	-	3.19	-	-	0.00	1.81	-	-
Zn	0.11	-	-	-	-	-	-	0.01	-	-
TOTAL	3.02	2.00	11.02	19.97	16.03	16.04	100.71	15.73	4.01	3.04
%XMg			84.4		33.4	34.2	-	63.6	59.7	

Table 3.3 Representative microprobe analyses of minerals in sample 257.

wt%	Spl	Crd	Kfs	Grt (core)	Grt (rim)	Sil (S_{2b})	Bt (S_{2b})
SiO_2	-	49.38	65.56	37.58	36.23	37.29	36.84
TiO_2	-	-	-	-	-	-	3.61
Al_2O_3	61.30	33.8	18.75	23.03	23.54	61.67	17.12
Cr_2O_3	0.35	-	-	-	-	-	-
FeO	26.55	5.07	-	32.06	32.21	1.16	15.65
MnO	0.59	0.28	-	1.11	1.08	-	0.12
MgO	7.98	10.39	-	7.9	8.17	-	14.04
CaO	-	-	0.14	0.13	0.18	-	-
Na_2O	0.08	0.13	2.22	-	-	-	0.26
K_2O	-	-	13.06	-	-	-	8.73
ZnO	6.04	-	-	-	-	-	-
TOTAL	102.89	99.05	99.73	101.8	101.41	100.12	96.37
Structural analysis							
basis of	32 (O)	18 (O)	32 (O)	24 (O)	24 (O)	5 (O)	22 (O)
Si	-	4.98	12.00	5.80	5.64	1.01	5.43
Ti	-	-	-	-	-	-	0.40
Al	15.61	4.01	4.04	4.18	4.31	1.99	2.97
Cr	0.06	-	-	-	-	-	-
Fe	4.80	0.43	-	4.14	4.19	0.03	1.93
Mn	0.11	0.02	-	0.15	0.14	-	0.02
Mg	2.57	1.56	-	1.82	1.90	-	3.08
Ca	-	-	0.03	0.02	0.03	-	-
Na	0.33	0.03	0.79	-	-	-	0.07
K	-	-	3.05	-	-	-	1.64
Zn	0.97	-	-	-	-	-	-
TOTAL	24.16	11.025	19.90	16.10	16.203	3.00	15.54
%XMg		78.50		30.50	31.10		61.5

Table 3.4 Representative microprobe analyses of cordierite and M_2 symplectite in sample 702.

wt%	Crd	Crd	Opx (M_2)	Opx (M_2)	Sil (M_2)	Sill (M_2)	Bt (M_2)
SiO_2	49.55	50.64	49.36	49.64	38.09	38.6	38.48
TiO_2	-	-	-	-	-	-	3.34
Al_2O_3	33.58	34.17	6.61	6.36	59.29	60.46	16.76
FeO	5.63	3.95	25.41	24.64	2.7	2.36	14.9
MnO	-	0.12	0.5	0.46	-	-	-
MgO	10.18	11.47	19.09	19.75	1.32	0.96	15.24
Na_2O	0.09	0.09	-	-	-	-	0.23
K_2O	0.07	-	-	-	-	-	9.04
TOTAL	99.1	100.44	100.97	100.85	101.4	102.38	97.99
Structural analysis							
basis of	18 (O)	18 (O)	6 (O)	6 (O)	5 (O)	5 (O)	22 (O)
Si	5.00	5.00	1.85	1.85	1.03	1.03	5.54
Ti	-	-	-	-	-	-	0.36
Al	3.99	3.97	0.29	0.28	1.88	1.90	2.84
Fe	0.48	0.33	0.79	0.77	0.06	0.05	1.79
Mn	-	0.01	0.02	0.02	-	-	-
Mg	1.53	1.69	1.06	1.10	0.05	0.04	3.27
Na	0.02	0.02	-	-	-	-	0.06
K	0.01	-	-	-	-	-	1.66
TOTAL	11.02	11.02	4.01	4.01	3.03	3.02	15.53
%XMg	76.3	83.8	57.3	58.8	46.6	42.2	64.6

As a consequence of these potential difficulties, the most successful calculations were obtained on S_2 assemblages, these minerals defining the main penetrative foliation (Tables 3.5). Using all S_2 mineral endmembers in sample 704, yielded P = 5.4±0.9 kbar (all ± at 2σ) at 750°C and a_{H_2O} = 0.3, but the calculation may be improved by excluding eastonite (on the basis of the diagnostics, Powell and Holland, 1988), to arrive at P = 5.1±1.0 kbar with σfit = 1.3. Also excluding eastonite from the calculations, the effect of a_{H_2O} can be considered. There is a moderate pressure dependence on a_{H_2O}, with average pressure decreasing with decreasing a_{H_2O} (Table 3.5). However, all calculations are within statistical error of each other, and σfit is minimized for low a_{H_2O} (Table 3.5), consistent with the rocks being at granulite facies. Although the calculations turn out to be weakly dependent on temperature (e.g. Table 3.5), a temperature of 750°C is used in this section because, this is the preferred temperature of similar spinel-bearing mineral assemblages elsewhere (Stüwe and Powell, 1989a, 1989b).

Calculations using S_2 assemblages in sample 257 gave a similar result to sample 704, yielding P = 6.0±0.70 kbar for 750°C and a_{H_2O} = 0.3. Eastonite was excluded on the basis of diagnostics (Table 3.5). Hence, D_2 in the Strangways Metamorphic Complex is inferred to occur at pressures between 4 and 6 Kbar, consistent with calculations on similar spinel-bearing assemblages from elsewhere (Stüwe and Powell, 1989a, 1989b). From arguments presented in the previous section, peak metamorphic conditions probably occurred at higher temperatures than S_2 assemblages and at similar pressures. Scapolite-wollastonite-grossular-anorthite assemblages in calc-silicate rocks imply a high temperature at peak metamorphism (>850°C, Chapter 4), higher than that for S_2 assemblages. Experiments by Richardson (1968) also imply low pressures at these temperatures for hercynitic spinel-quartz assemblages at peak metamorphism, consistent with the average pressure calculations. The presence of cordierite-quartz-K feldspar in S_2 leucosome layers and spinel inclusions in cordierite are also indicative of low pressure conditions (Seifert, 1974). Using the stability data of Hensen and Green (1973) for cordierite and garnet (CAGS geobarometer), an upper pressure of 6 kbar is obtained for D_2 confirming the average pressure calculations. The calculated pressures are

Table 3-5 Average pressure calculations on the mineral parageneses in samples 704, 257 and 702, following the approach of Powell and Holland (1988) with the expanded internally consistent dataset of Holland and Powell (1990).

S_2 assemblage in sample 704: Grt-Bt-Crd-Spl-Sil gneiss

Endmembers	phl	ann	east	naph	crd	fcrd	py	alm	ab	ksp	sp	herc	q	sill
Activities (a)	0.156	0.012	0.032	0.031	0.636	0.034	0.033	0.255	0.563	0.789	0.34	0.65	1.0	1.0
σ (ln a)	0.220	0.534	0.406	0.324	0.040	0.399	0.415	0.121	0.057	0.013	0.131	0.037	0	0

Independent reactions — Calculated pressures at T=750°C and a (H_2O) = 0.3

	P(T)	σ	dT/dP	ln K
1) py + 2sill = crd + sp	4.9	0.68	0.0023	1.877
2) 3alm + 6sill = 2fcrd + 5herc + 5q	5.7	0.62	0.0107	-4.805
3) 9crd + 10herc + 10q = 5fcrd + 6py + 12sill	3.1	1.12	-0.0017	-28.946
4) 5phl + 6crd + 15herc + 15q = 5ann + 9py + 18sill	3.8	1.06	-0.0013	-34.280
5) 3east + 3py + 4herc + 4q = 3phl + 2fcrd + 6sp	1.4	1.64	-0.0032	3.514
6) 5naph + 6crd + 5ksp + 15herc + 15q = 5ann + 9py + 5ab + 18sill	4.0	1.08	-0.0004	-27.872

Average pressures — all endmembers / excluding eastonite

T°C	700	750	800		700	750	800	
av. P (kbar)	5.0	5.4	5.7		4.7	5.1	5.4	
σ	0.86	0.90	0.94		0.46	0.50	0.55	
σfit	2.3	2.3	2.3		1.2	1.3	1.3	

The effect of varying a (H_2O) (at T=750°C and without eastonite)

a (H_2O)	P±2σ	σfit	
0.1	4.76±0.9		1.14
0.3	5.06±1.0		1.27
0.5	5.34±1.2		1.38
0.7	5.59±1.2		1.49

S_2 assemblage in sample 257: Grt-Bt-Crd-Spl-Sil gneiss

Endmembers	phl	ann	east	py	alm	ksp	crd	fcrd	sp	herc	q	sill
Activities (a)	0.117	0.011	0.055	0.041	0.242	0.789	0.599	0.041	0.360	0.580	1.0	1.0
σ (ln a)	0.260	0.541	0.351	0.385	0.128	0.014	0.048	0.381	0.122	0.053	0	0

Independent reactions — Calculated pressures at T=750°C and a (H_2O) = 0.3

	P(T)	σ	dT/dP	ln K
1) fcrd + herc = alm +2sill	6.3	0.63	0.0104	2.318
2) 3crd + 3herc = 2py + alm + 6sill	5.7	0.44	0.0048	-4.616
3) 9py + 10q + 18sill = 11crd +5sp	5.7	0.55	0.0032	17.915
4) 5east +4crd = 5phl +py +12sill	8.5	1.09	0.0099	2.622
5) ann + crd = east +alm + 3q	4.7	1.10	0.0082	0.671

Average pressures — all endmembers / excluding eastonite

T°C	700	750	800	850	900		700	750	800	850	900
av P (kbar)	5.7	6.1	6.4	6.7	7.0			5.7	6.0	6.3	6.6
σ	0.43	0.46	0.51	0.57	0.64			0.33	0.35	0.36	0.40
σfit	1.3	1.3	1.4	1.5	1.6			0.6	0.7	0.8	1.1

The effect of varying a (H_2O) at T=750°C and without eastonite

a (H_2O)		P±2σ	σfit	
	6.9	0.1	5.54±0.7	0.56
	0.50	0.3	5.97±0.7	0.67
	1.3	0.5	6.36±0.7	0.79
		0.7	6.72±0.7	0.90

M_2 assemblage in sample 702: Opx-Bt-Sil symplectites

Endmembers	phl	ann	east	naph	crd	fcrd	py	alm	ab	ksp	en	fs	mgts	q	sill
Activities (a)	0.111	0.026	0.044	0.027	0.547	0.591	0.033	0.255	0.563	0.789	0.306	0.125	0.073	1.0	1.0
σ (ln a)	0.267	0.445	0.375	0.366	0.062	0.344	0.415	0.121	0.057	0.013	0.145	0.251	0.258	0	0

Independent reactions — Calculated pressures at T=800°C and a (H_2O) = 0.5

	P(T)	σ	dT/dP	ln K
1) 2py + 3q = crd + 2en	4.6	1.31	-0.0021	3.845
2) 3crd = 2py + 5q + 4sill	6.6	0.54	0.0039	-5.007
3) 3fcrd = 2alm +5q + 4sill	7.1	0.64	0.0099	5.753
4) phl + crd = east + py + 3q	3.9	1.17	-0.0015	-3.728
5) 5naph + 6crd = 9py + 5ab + 3sill + 5H2O	5.1	1.26	-0.0112	-11.92
6) 5phl +6crd = 9py + 5ksp +3sill + 5H2O	5.2	1.25	-0.0126	-17.248
7) 4ann + 3fcrd + 3q = 6alm + 4ksp + 4H2O	4.5	1.29	-0.0039	13.907
8) 3east + 3fs + 3mgts + 9q = phl +2ann +3crd	4.5	1.39	-0.0018	12.166

Average pressures — all endmembers / excluding eastonite

T°C	700	750	800	850	900		700	750	800	850	900	
av P (kbar)	6.5	7.0	7.4	7.8	8.2			6.6	7.1	7.5	7.9	8.3
s	0.62	0.50	0.45	0.46	0.49			0.53	0.41	0.39	0.44	0.49
sfit	2.5	2.0	1.7	1.8	1.9			2.1	1.6	1.5	1.7	1.8

The effect of varying a (H_2O) at T=800°C and without eastonite

a (H_2O)	P±2σ	σfit	
0.1	7.25±1.9		3.58
0.3	7.18±1.0		1.84
0.5	7.50±0.78		1.49
0.7	7.79±0.80		1.54

significantly lower than initial pressures of 8±1 kbar inferred by Warren (1982, 1983a) for the Strangways Metamorphic Complex. Oliver et al. (1988) have also inferred lower initial pressures than Warren (1982,1983a) but did not recognize any subsequent increase in pressure.

Estimates for M_2 conditions were obtained using a pseudomorphous, symplectic sillimanite-orthopyroxene aggregate in sample 702 (Table 3.5). Average pressure calculations yielded P = 7.5±0.8 kbar at 800°C and a_{H_2O} = 0.5, and σfit = 1.5 when eastonite was excluded on the basis of the diagnostics. Excluding eastonite, the average pressure calculations show only a weak dependence on a_{H_2O} (Table 3.5) but with σfit minimized for a_{H_2O} = 0.5. Omitting eastonite from the calculations, the effect of temperature may be considered: average pressures increasing with increasing temperature, but with σfit minimized for a temperature of 800°C (Table 3.5).

In conclusion, the average pressure calculations are consistent with D_2 occurring at 5.5±0.8 kbar and at temperatures of 750°C. Calc-silicate assemblages suggest that peak metamorphic temperatures were greater than 850°C. The texturally-distinct, post S_2 sillimanite-orthopyroxene symplectites imply conditions of 7.5±0.8 kbar and 800°C for M_2. The inference that the M_2 assemblage occurs at higher temperatures than S_2 assemblages is consistent with the topology of the petrogenetic grid (Fig. 3.5). The reason higher temperature conditions did not erase evidence of the S_2 assemblages was presumably because there was an insufficient influx of water during D_3 to enable M_2 to establish the dominant mineral assemblage in the Strangways Metamorphic Complex. The quantitative estimates of metamorphic conditions confirm the P-T path qualitatively outlined by the crossing of univariant reactions on the petrogenetic grid.

3.5 Discussion

3.51 A P-T-t path for the Strangways Metamorphic Complex

The P-T path outlined above for the Strangways Metamorphic Complex (Fig. 3.5) is complimentary to the work of Warren (1982, 1983a), as summarized in Table 3.1.

However, in this chapter an early, low-pressure metamorphism (M_1), characterized by spinel-quartz-bearing assemblages is inferred from metapelites. Approximate isobaric cooling from peak M_1 conditions occurred at P = 5.5±0.8 kbar, during D_2 that produced the main penetrative foliations in the terrain, S_1 and S_2. Assemblages in Division 1, metapelitic rocks from the Reynolds Range area, 150 km northwest of the Strangways Range, also suggest lower initial pressures (< 6 kbar, Warren and Stewart, 1988) as part of an anticlockwise P-T-t path. The ~1800 Ma Rb-Sr age of Black et al. (1983), which they relate to a early granulite facies metamorphism called the Strangways Event and the granulite facies Arunta Orogeny of Allen and Stubbs (1982), most probably coincide with M_1 in this chapter. An initial stage of cooling was referred to by Warren (1982, 1983a) as the "biotite stage", and probably corresponds to the cooling from M_1 during which the coarse-grained sillimanite S_{2b} folia formed. There is some overlap of the granulite and biotite stages of Warren (1983a) because of the interpretation of cooling during D_2 from M_1, at granulite facies conditions (see Table 3.1).

Compression during D_3, which produced isoclinal to open, inclined F_3 and F_4 folds, resulted in the Strangways Metamorphic Complex being buried to M_2 conditions of P = 7.5±0.8 kbar. The early D_3 folds appear to have been mylonitic with their fold axes parallel to the stretching lineations (Chapter 2). Cordierite in the metapelitic gneisses was partially to completely pseudomorphed by orthopyroxene-sillimanite -biotite-magnetite symplectites. Allen and Stubbs (1982) inferred an age of 1470±60 Ma for the development of symplectic aggregates similar to the M_2 symplectite described in this chapter.

From a study of rocks in the northern Strangways Range, 50 km north-west of this study area, Warren (1982, 1983a) estimated peak metamorphic pressure-temperature conditions to be 8±1 kbar at 850-920°C from calculations based on a comparison of garnet-cordierite-orthopyroxene-quartz assemblages, co-existing pyroxene and clinopyroxene-plagioclase-quartz assemblages. Warren (1982, 1983a) only reports fine-grained orthopyroxene-sillimanite intergrowths, which replace cordierite, after the biotite

stage, as part of an isobaric cooling path. Windrim (1983) also estimated similar peak metamorphic conditions of 8 kbar and 840°C for rocks from the Strangways Range. Warren (1982,1983a) postulated near isobaric cooling to the kyanite field from this "initial" moderate-pressure metamorphic event, during which there was hydration of the high-grade assemblages: biotite formed from the hydration of orthopyroxene and garnet in felsic granulites, and pargasitic hornblende formed around the rims of orthopyroxene in metabasic rocks. These peak metamorphic pressure estimates are significantly higher than estimates in this chapter but within statistical error of estimates for M_2. It is possible that pressure estimates by Warren (1982, 1983a) and Windrim (1983) reflect conditions during a major reworking of the terrain during D_3/M_2.

Kyanite±gedrite±staurolite-bearing rocks, suggesting conditions of ~8 kbar, are observed in south-directed shear zones similar to those that bound the Ongeva granulites and the Anamarra granite domain, and are assigned to the kyanite-gedrite stage (Warren, 1983a, Table 3.1). This probably corresponds to D_5 in Chapter 2. D_4 ultramylonitization certainly predates D_5 thrusting on the northern margin of the Strangways Metamorphic Complex and hence the "kyanite-gedrite stage" of Warren (1983a). Conditions of D_4 were probably not far removed from M_2, as indicated by the neocrystallization of sillimanite and biotite and recrystallization of orthopyroxene, clinopyroxene and garnet in the ultramylonite zones (Chapter 5). D_4 ultramylonitization is placed into the P-T frame-work in Chapter 5.

Later cordierite coronas on kyanite and sillimanite in kyanite±gedrite±staurolite-bearing shear zones imply some isothermal uplift (Warren, 1983a) from these conditions. Pb/U zircon data yield isotopic ages of ~1750 Ma (Mortimer et al., 1987, Cooper et al., 1988) for crystallization of the Bruna Gneiss, which according to Ding and James (1985) and James and Ding (1988) intruded along a thrust contact between the Harts Range Group and the Strangways Metamorphic Complex. These data imply that thrusting occurred at ~1750 Ma and are in conflict with the ~1470 Ma dates for M_2 (Allen and Stubbs, 1982). Evidence presented in this chapter shows that M_2 occurred before D_4

ultramylonitization and D_5 thrusting. The petrological effects of the kyanite-gedrite stage and subsequent isothermal decompression (Warren, 1983a) were not observed in the mineral assemblages from the discrete morphological units within the Strangways Metamorphic Complex. Hence, the interpretation of the P-T evolution of the Strangways Metamorphic Complex after D_4 relies upon the work of Warren (1982, 1983a).

3.52 The tectonic setting of M_1 and M_2

The inferred metamorphic history for the Strangways Metamorphic Complex contrasts with that of Warren (1982, 1983a), and is different to the inferred metamorphic history of most granulite terrains in the world, which record evidence for either isobaric cooling or isothermal uplift (Harley, 1989). An increase in pressure has been inferred for a prograde and retrograde path in the Namaqualand Metamorphic Complex, South Africa (Waters, 1986) but was explained by the addition of felsic magmas. A cooling path with a slight-increase in pressure was also inferred for granulites from Labwor Hills, Uganda (Sandiford et al., 1987) but due to the lack of evidence for decompression the crust was assumed to be of normal thickness and the slight increase in pressure was not due to tectonism. In this chapter, evidence is presented for a significant increase in pressure after the metamorphic peak, at granulite facies conditions, which was probably associated with a major deformation. This deformation may represent a crustal thickening event, in the Strangways Metamorphic Complex during the early- to mid-Proterozoic, similar to a collisional-style of tectonics.

Due to the extensive disruption of the Strangways Metamorphic Complex by younger retrograde shear zones and, in particular, the destruction of primary sedimentary features by recrystallization during M_1, many tectonic constraints are lost. However, M_1 has features typical of low-pressure granulite facies metamorphisms elsewhere (e.g. Hobbs et al., 1984; Sandiford, 1985b; Clarke et al., 1987, 1989) and is of similar, though poorly constrained, age to major metamorphic events in the Reynolds Range-Anmatjira Range region (Collins et al., 1991). The peak metamorphic events in the Reynolds Range-Anmatjira Range region appear to cause only minor disruption to

regional stratigraphy. Mapped isograds also transgress stratigraphic and deformation surfaces in each metamorphism (Clarke et al., 1989). Although the immediate cause of the thermally perturbed metamorphisms in the Reynolds Range-Anmatjira Range involved advection (Vernon et al., 1990), the ultimate cause of metamorphism was probably asthenospheric thermal perturbations. A similar setting for M_1 in the Strangways Metamorphic Complex is also inferred.

The *up-pressure* M_2 metamorphism associated with D_3 in the Strangways Metamorphic complex may be explained by: lithospheric loading on a thinned crust (e.g. Sandiford and Powell, 1986); tectonic thickening due to overthrusting; the thrusting of the rocks deeper into the crust; or the addition of voluminous acid magmas to the crust. Given that D_3 was a major folding episode it seems likely that tectonic processes were responsible for the increase in pressure. The absence of high-pressure, blue-schist facies assemblages in the Arunta Block would tend to suggest an increase in pressure due to overthrusting, rather than underthrusting in a subduction environment. Nevertheless, this increase in pressure is equivalent to a crustal thickening of 8 to 9 km which occurred prior to the Kyanite-gedrite stage of Warren (1983a). These rocks would have been near the base of a continental crust of normal thickness, or in the middle of an over-thickened crust at the end of D_2. From evidence in the Anmatjira-Reynolds Range area (Clarke et al., 1990) and the inferred isobaric cooling path for M_1, it seems likely that the M_2-D_3 event was independent of the processes responsible for M_1-D_1/D_2. If so, M_2 metamorphism must be placed in a tectonic setting entirely unlike that inferred by Warren (1983a) and quite unlike the setting for M_1. The increase in pressure during M_2 is similar to the effect produced by continental collision in modern orogenic belts (e.g. Selverstone et al., 1984), from which a clockwise P-T-t path has been inferred.

There is no estimate of the absolute time involved between metamorphisms, nor of the age of D_4 ultramylonites or rocks of the kyanite-gedrite stage. However, the data of Windrim and McCulloch (1986) and Mortimer et al. (1987) suggest only a short period (about 250 Ma) between crustal formation and D_5 thrusting. The D_4

ultramylonites may record a continuation of the thermally-perturbed conditions that caused M_2, and could be an extensional response to crustal thickening during D_3 (c.f. Selverstone, 1988, Norman, 1989). However, if we accept the pressure estimate of Warren (1983a) for the initial kyanite-gedrite stage, even taking errors into account, any uplift during D_4 is limited. It is conceivable that D_5 shearing is a also continuation of the tectonism associated with M_2/D_3. Warren (1983a) has observed cordierite overgrowths on kyanite within the D_5 shear zones which infers some isothermal uplift after the kyanite-gedrite stage probably due to isostatic adjustment of an over-thickened crust. Of course, it is entirely conceivable that either, or both, of D_4 and the kyanite-gedrite (D_5) stages are unrelated to collisional orogens and to M_2.